




An RDH-Plin2 axis modulates lipid droplet size by antagonizing Bmm lipase

Xuefan Zhao^{1,2} , Wei Wang¹, Yan Yao¹, Xia Li¹ , Xiahe Huang¹, Yingchun Wang¹, Mei Ding¹ & Xun Huang^{1,2,*} 

Abstract

The size of lipid droplets varies greatly *in vivo* and is determined by both intrinsic and extrinsic factors. From an RNAi screen in *Drosophila*, we found that knocking down subunits of COP9 signalosome (CSN) results in enlarged lipid droplets under high-fat, but not normal, conditions. We identified CG2064, a retinol dehydrogenase (RDH) homolog, as the proteasomal degradation target of CSN in regulating lipid droplet size. RDH/CG2064 interacts with the lipid droplet-resident protein Plin2 and the RDH/CG2064-Plin2 axis acts to reduce the overall level and lipid droplet localization of Bmm/ATGL lipase. This axis is important for larval survival under prolonged starvation. Thus, we discovered an RDH-Plin2 axis modulates lipid droplet size.

Keywords ATGL; large lipid droplet; RDH/Plin2

Subject Categories Membranes & Trafficking; Post-translational Modifications & Proteolysis

DOI 10.15252/embr.202152669 | Received 12 February 2021 | Revised 4 December 2021 | Accepted 21 December 2021 | Published online 8 February 2022
EMBO Reports (2022) 23: e52669

Introduction

Cellular neutral lipids, such as triglyceride (TAG), are mainly stored in the form of lipid droplets with a neutral lipid core covered by a phospholipid monolayer coated with various proteins. The size and the number of lipid droplets determine the cellular capacity for lipid storage. In terms of lipolysis, large lipid droplets are relatively inactive compared with small lipid droplets. Under lipid-overload conditions, the formation of large lipid droplets is beneficial to reduce lipotoxicity caused by excess lipids (Farese & Walther, 2009; Walther & Farese, 2012; Kraemer *et al*, 2013; Gluchowski *et al*, 2017; Yu & Li, 2017; Chen *et al*, 2019).

Lipid droplet size is determined by three factors: the neutral lipid content, the composition of the phospholipid monolayer, and the action of lipid droplet-associated proteins. Excess cellular energy, in the form of fatty acids or of glucose, which can be converted to fatty

acids through glycolysis and *de novo* lipogenesis, can be stored through increasing the neutral lipid content and the expansion of lipid droplets (Ruggles *et al*, 2013; Welte, 2015; Ding *et al*, 2018). Phosphatidylcholine (PC) and phosphatidic acid (PA) regulate lipid droplet size by affecting the membrane curvature and the coalescence of lipid droplets, respectively (Guo *et al*, 2008; Fei *et al*, 2011). Some lipid droplet-associated proteins, such as DGAT2, CCT1, and GPAT4, are able to change the neutral lipid content and the composition of the phospholipid monolayer through local synthesis of phospholipids or TAG (Wilfling *et al*, 2013). In addition, other lipid droplet-associated proteins, such as Fsp27, PLIN2, and PLIN5, affect lipid droplet size through regulating lipid droplet fusion, lipolysis or lipid droplet contacts with other organelles such as mitochondria or peroxisomes (Listenberger *et al*, 2007; Guo *et al*, 2008; Fei *et al*, 2011; Gong *et al*, 2011; Wang *et al*, 2011; Li *et al*, 2017; Kong *et al*, 2020). Despite this rapidly growing knowledge, the activities of lipid droplet-associated proteins and the mechanisms that regulate them are far from clear.

Heterogeneity, both intercellular and intracellular, is an important but poorly studied feature of lipid droplets (Rinia *et al*, 2008; Herms *et al*, 2013). The variation in size represents just one type of lipid droplet heterogeneity. Lipid droplets may contain different neutral lipids, such as TAG, cholesterol ester (CE), or retinyl ester (RE), and these neutral lipids may also differ in the saturation of their fatty-acyl chains (Blaner *et al*, 2009; Molenaar *et al*, 2017; Pacia *et al*, 2020). The composition of lipid droplet-associated proteins also varies greatly, and this contributes significantly to lipid droplet dynamics (Rinia *et al*, 2008). Moreover, lipid droplets can even have heterogeneous origins. For example, lipid droplets in *Drosophila* fat cells can be classified into two subgroups (Diaconeasa *et al*, 2013; Ugrankar *et al*, 2019). One subgroup is called peripheral lipid droplets, which are small and near the cell surface. Peripheral lipid droplet formation depends on exogenous lipids transported from the intestine to adipose tissue. The other subgroup is medial lipid droplets, which originate from the peri-nuclear endoplasmic reticulum (ER). Their formation and growth mainly rely on *de novo* fatty acid synthesis. Although the heterogeneous aspects of lipid droplets are well-recognized, the regulation and coordination of different subpopulations of lipid droplets have not been well studied.

1 State Key Laboratory of Molecular Developmental Biology, Institute of Genetics and Developmental Biology, Innovation Academy for Seed Design, Chinese Academy of Sciences, Beijing, China

2 University of Chinese Academy of Sciences, Beijing, China

*Corresponding author. Tel./Fax: 86 10 64806560; E-mail: xhuang@genetics.ac.cn

Here, we report a retinol dehydrogenase (RDH)/CG2064-Plin2-Bmm axis which regulates lipid droplet size under high-fat conditions. RDH/CG2064 directly interacts with Plin2. Increasing the level of RDH/CG2064 changes the localization of Plin2 from peripheral lipid droplets to small lipid droplets around the nucleus and also reduces the level and lipid droplet localization of Bmm lipase. The reduction of Bmm results in large lipid droplets under high-fat conditions. Finally, this axis maintains larval survival under prolonged starvation.

Results

COP9 signalosome complex regulates lipid droplet size under high-fat conditions

To study lipid storage regulation, we previously used *pumpless-GAL4* (*ppl-GAL4*)-driven gene overexpression or knockdown in *Drosophila* 3rd instar salivary gland and fat body (Liu *et al*, 2014; Fan *et al*, 2017; Yao *et al*, 2018). Interestingly, overexpressing *DGAT1* (*ppl>DGAT1*), which encodes a diacylglycerol O-acyltransferase for TAG biosynthesis, did not lead to significantly enlarged lipid droplets in 3rd instar larval fat body. The overall level of TAG is only marginally increased (Fig 1A and B). Besides genetic manipulation, we also reared larvae on a 30% coconut oil-containing high-fat diet. The expression of *DGAT1* increases 2.8 fold under high-fat feeding (Fig EV1A). However, similar to *DGAT1* overexpression (OE), the high-fat diet did not increase lipid droplet size in 3rd instar larval fat body (Fig 1C). In addition, the combination of high-fat diet and *DGAT1* overexpression did not dramatically increase lipid droplet size compared with *DGAT1* overexpression alone (Fig EV1B).

To investigate why these high-fat conditions did not result in large lipid droplets, we conducted an RNAi screen in the *ppl>DGAT1* background. We found that RNAi of *CSN3* led to significantly enlarged lipid droplets in 3rd instar larval fat body (Fig 1D and E). Constitutively photomorphogenic 9 (COP9) signalosome (CSN) is an eight-subunit protein complex that modulates the activity of an E3 ubiquitin ligase, Cullin-Ring Ligase (CRL), by removing the ubiquitin-like molecule Nedd8 from Cullin (Craney & Rape, 2013). We then examined whether RNAi of other CSN subunits phenocopies *CSN3* RNAi. RNAi knockdown of several other CSNs, including *CSN2*, *CSN5*, or *CSN7*, results in enlarged lipid droplets in *ppl>DGAT1* 3rd instar larval fat body (Fig 1D and E). Consistent

with the increased lipid droplet size, the level of TAG is increased in *CSN2* RNAi with *DGAT1* OE compared with *DGAT1* OE alone (Fig 1B).

Since we identified *CSN3* in the *DGAT1* OE background, we then tested whether CSN regulates lipid storage and lipid droplet size under normal conditions. In 3rd instar larval fat body, *CSN2* RNAi slightly, but not significantly, increased the TAG level (Fig 1B), and it had no effect on lipid droplet size (Fig 1D and E). Similarly, RNAi of other CSN subunits did not increase the lipid droplet size (Fig 1D and E), which suggests that regulation of lipid droplet size by CSN depends on high-fat conditions. Indeed, *CSN3* RNAi also increased the lipid droplet size of 3rd instar larval fat body when the animals were fed on a 30% coconut oil-containing high-fat diet (Fig 1F and G). Together, these results demonstrate that CSN plays an important role in regulating lipid droplet size under high-fat conditions.

CSN-mediated protein degradation regulates lipid droplet size

CSN regulates CRL-mediated protein degradation by deneddylating Cullin. Since RNAi of the deneddylase *CSN5* affects lipid droplet size (Fig 1D and E), we speculated that CSN may regulate lipid droplet size through modulating CRL-mediated protein degradation. Therefore, we examined the lipid droplet phenotype of *Cullin* knockdowns under high-fat conditions. There are five *Cullin* genes in *Drosophila*. RNAi of *Cullin1*, 2, 3, or 5 did not affect lipid droplet size in 3rd instar fat body of *DGAT1* OE larvae (Fig EV1C and D), which suggests that these genes are unlikely to be involved in CSN-mediated lipid droplet size regulation. *ppl-GAL4*-driven *Cullin4* RNAi results in early larval lethality, which prevents us from directly observing the lipid droplet phenotype in 3rd instar larvae. To circumvent the early lethality barrier, we used a repressible binary expression *GAL4/GAL80* system to temporally control *Cullin4* RNAi. We grew *Tub-GAL80^{ts}*, *ppl>Cullin4* RNAi animals at 18°C to lower the RNAi efficiency and shifted the temperature to 29°C at 96 h after egg laying to activate the RNAi effect. With that manipulation, we found large lipid droplets in 3rd instar fat body of *Cullin4* RNAi larvae fed on a high-fat diet (Fig EV1E and F), which suggests that *Cullin4* is important for lipid droplet size regulation.

Depletion of *CUL4* and its “negative” regulator CSN induce the same phenotype. This apparent conflict is not surprising, because the neddylation-de-neddylation cycle is essential to maintain proper CRL function and disrupting the cycle often leads to a loss-of-function phenotype (Schwechheimer *et al*, 2001; Pierce *et al*, 2013; Bagchi *et al*, 2018). Along the same line, similar to the *Cullin4*

Figure 1. The CSN complex regulates lipid droplet size under high-fat conditions.

3rd instar larval fat bodies were stained by BODIPY (green) for lipid droplets and DAPI (blue) for nuclei. Scale bars represent 25 μm.

A Top: schematic diagram of the TAG biosynthetic pathway. Bottom: overexpression of *DGAT1* (*ppl>DGAT1*) does not affect lipid droplet size.

B Relative TAG levels in different genetic backgrounds were measured by glyceride assay kit. For quantification, TAG levels were normalized to protein. Error bars represent ± SEM. ****P* < 0.001; NS: non-significant.

C The lipid droplet size is not increased when larvae are reared on a 30% high-fat diet.

D *CSN* RNAi alone does not affect lipid droplet size, but *CSN* RNAi dramatically increases the lipid droplet size when *DGAT1* is overexpressed.

E Quantification of the lipid droplet size in (A) and (D).

F Lipid droplet size is increased in *CSN7* RNAi larvae fed on a 30% high-fat diet.

G Quantification of the lipid droplet size in (C and F). ND: normal diet; HFD: high-fat diet.

Data information: In (E) and (G), data were analyzed by one-way ANOVA with a *post hoc* Turkey's multiple-comparison test. Each point represents data from one fat body, and at least 30 cells were analyzed for each fat body. Error bars represent ± SEM. ****P* < 0.001; ***P* < 0.01; and NS: non-significant.

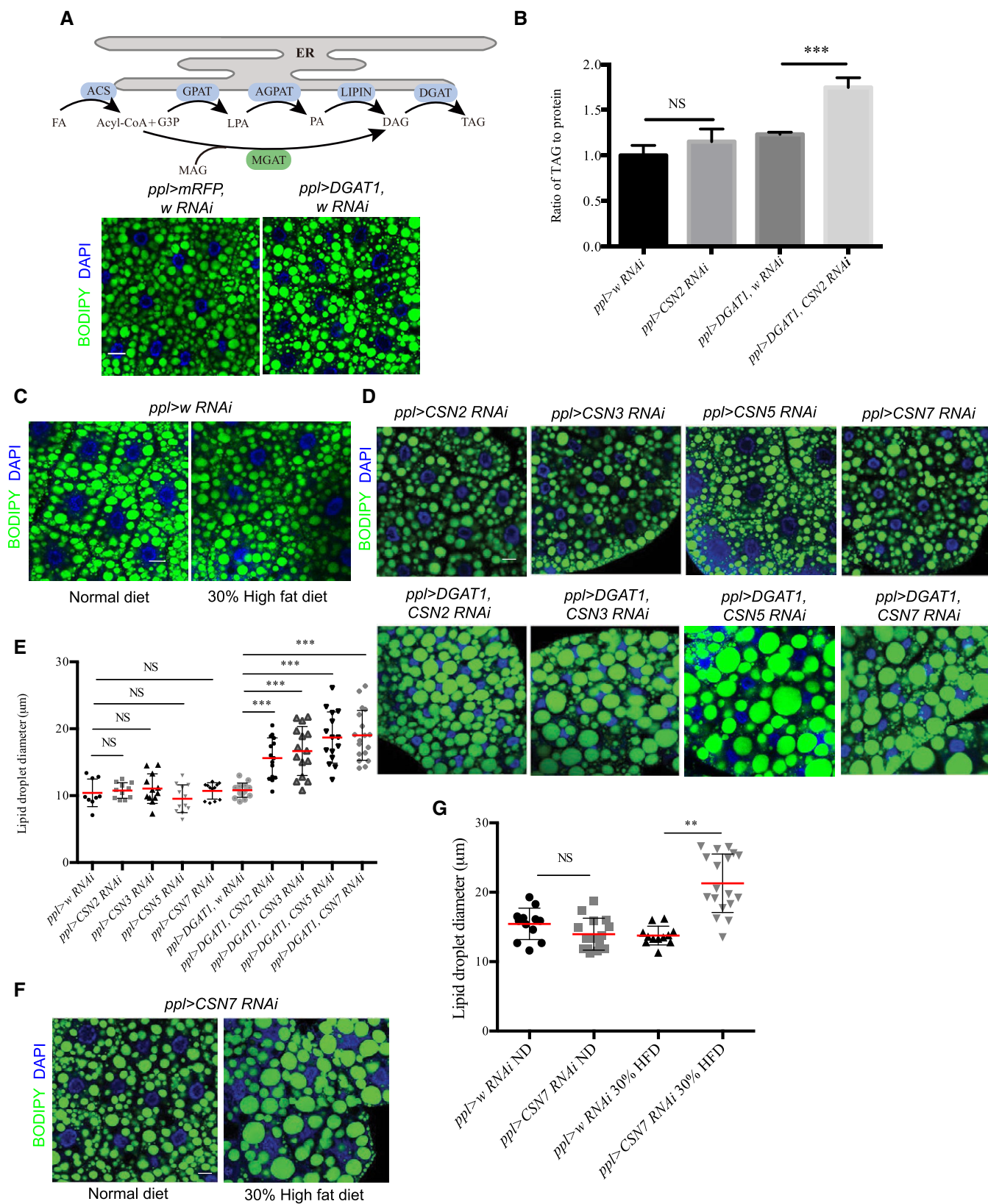


Figure 1.

RNAi/high-fat diet combination, lipid droplet size is increased in 3rd instar fat body of *DGAT1* OE larvae with *Cand1* RNAi (Fig EV1G and H). *Cand1* is a key player in recycling NEDD8 from CRL (Min et al, 2003). Loss of *Cand1* impairs CRL-mediated protein degradation and mimics CSN knockdown. Taken together, these results indicate that CSN-mediated protein degradation regulates lipid droplet size under high-fat conditions.

CSN regulates lipid droplet size through degrading CG2064, an RDH homolog

To identify downstream target(s) of CSN in this process, we performed comparative quantitative proteomic analysis on fat body samples from animals overexpressing *DGAT1* alone (control), and overexpressing *DGAT1* with *CSN2* RNAi or *CSN7* RNAi (Dataset EV1). We identified ~3,000 proteins from the proteomic analysis and we plotted the proteins according to the logarithm-transformed ratios of different samples and *P*-values. We focused on proteins with a *P* value below 0.05 and with a fold change of over 1.5 or below 0.67. With this standard, there are 131 up-regulated proteins and 66 down-regulated proteins in *CSN2* RNAi compared with control, and 121 up-regulated proteins and 66 down-regulated proteins in *CSN7* RNAi compared with control (Fig 2A). There are 90 up-regulated proteins and 45 down-regulated proteins in common between *CSN2* RNAi and *CSN7* RNAi samples (Fig 2A).

We further examined the molecular functions of proteins in the overlapping group and performed a literature search for potential lipid links. This led us to four up-regulated proteins (CG2064, CG2065, CG9360, and *Arc1*) and three down-regulated proteins (*Pka-R1*, CG18135, and CG4500) (Fig 2A). CG2064, CG2065, and CG9360 belong to the NADP(H)-dependent short-chain dehydrogenase/reductase (SDR) family and are up-regulated more than 3-fold in *CSN2* or *CSN7* RNAi. SDR is a large protein superfamily and two SDR subfamilies, hydroxysteroid dehydrogenase (HSD) and RDH, have been reported to regulate lipid droplet dynamics (Deisenroth et al, 2011; Adams et al, 2014; Siddiqah et al, 2017; Yang et al, 2018). CG2064 and CG2065 belong to the RDH subfamily. *Arc1* is a cytoskeleton protein and the cytoskeleton regulates lipid droplet morphology (Mosher et al, 2015). *Pka-R1* is a cAMP-dependent protein kinase (PKA) regulator, and PKA is well known for its function in regulating lipase activity (Greenberg et al, 1991; Miyoshi

et al, 2007). CG18135 is a glycerophosphocholine phosphodiesterase and CG4500 is a long-chain fatty acid ligase.

To further evaluate these candidates, we manipulated their expression in different genetic backgrounds and examined the lipid droplet phenotype. Overexpression of *Arc1* and RNAi of *Pka-R1*, CG18135 or CG4500 did not lead to increased lipid droplet size (Fig EV2A). In addition, CG2065 RNAi or CG9360 RNAi did not rescue the enlarged fat body lipid droplet phenotype in 3rd instar *DGAT1* OE larvae with *CSN2* RNAi (Fig EV2B). These results suggest that these genes do not act downstream of CSN in regulating lipid droplet size. In contrast, CG2064 RNAi suppresses the large lipid droplet phenotype caused by *CSN2* RNAi in *DGAT1* OE larvae (Fig 2B and C). We observed a similar rescuing effect of CG2064 RNAi on *CSN2* RNAi with high-fat feeding (Fig 2B and C). These results suggest that CG2064 acts downstream of CSN to control lipid droplet size under high-fat conditions.

We therefore focused on CG2064. Since CG2064 has not been functionally studied before, we refer to it hereafter as RDH/CG2064. We expressed a C-terminal GFP-tagged RDH/CG2064 in *Drosophila* S2 cultured cells. Treatment with the proteasome inhibitor MG132 dramatically increased the level of RDH/CG2064-GFP in S2 cells (Fig 2D), which indicates that RDH/CG2064 can be degraded through the proteasome pathway. We also generated an RDH/CG2064-GFP knockin *Drosophila* reporter line and compared the level of RDH/CG2064-GFP by western blot analysis of 3rd instar fat body lysates of *DGAT1* OE larvae with and without *CSN2* RNAi. As expected, *CSN2* RNAi dramatically increases the level of RDH/CG2064-GFP (Fig 2E), which supports the hypothesis that CSN regulates RDH/CG2064 proteasomal degradation. Consistent with the post-transcriptional regulation of RDH/CG2064 by CSN, the mRNA level of *RDH/CG2064* in 3rd instar larval fat body is not significantly changed by *CSN2* RNAi (Fig EV3A). Together, these results indicate that CSN regulates lipid droplet size through proteasomal degradation of RDH/CG2064.

RDH/CG2064 overexpression increases lipid droplet size under high-fat feeding

Since CSN RNAi increased the RDH/CG2064 level and the lipid droplet size under high-fat conditions, we next investigated whether RDH/CG2064 overexpression is sufficient to increase lipid droplet

Figure 2. Elevating the level of RDH/CG2064 in CSN RNAi increases lipid droplet size.

- A The number of proteins changed in *CSN2* or *CSN7* RNAi revealed by quantitative proteomics. Red: the number of up-regulated proteins and green: the number of down-regulated proteins. Candidate proteins from the quantitative proteomics are listed along with protein fold changes in *CSN2* or *CSN7* RNAi. 3rd instar larval fat bodies were stained by BODIPY (green) for lipid droplets and DAPI (blue) for nuclei. Scale bars represent 25 μ m.
- B *RDH/CG2064* RNAi suppresses the enlarged lipid droplet phenotype in *CSN2* RNAi under *DGAT1* overexpression (*pp1>DGAT1*) or high-fat diet conditions.
- C Quantification of the lipid droplet size in (B). HFD: high-fat diet.
- D In *Drosophila* S2 cells expressing RDH/CG2064-GFP, treatment with the proteasome inhibitor MG132 increases the RDH/CG2064-GFP protein level detected by anti-GFP antibody in a western blot.
- E The RDH/CG2064-GFP protein level is increased in *pp1>DGAT1* larvae with *CSN2* RNAi, as detected by anti-GFP antibody in a western blot.
- F *RDH/CG2064* overexpression increases lipid droplet size in *pp1>DGAT1* larvae.
- G Quantification of the lipid droplet size in (F).
- H Relative TAG levels in different genetic backgrounds were measured by glyceride assay kit. For quantification, TAG levels were normalized to protein.
- I *RDH/CG2064* and *CG2065* deletion does not affect lipid droplet size under normal or high-fat diet conditions.

Data information: In (C), (G), and (H), data were analyzed by one-way ANOVA with a post hoc Turkey's multiple-comparison test. Each point represents data from one fat body, and at least 30 cells were examined in each fat body. Error bars represent \pm SEM. ****P* < 0.001; ***P* < 0.01; and NS: non-significant.

Source data are available online for this figure.

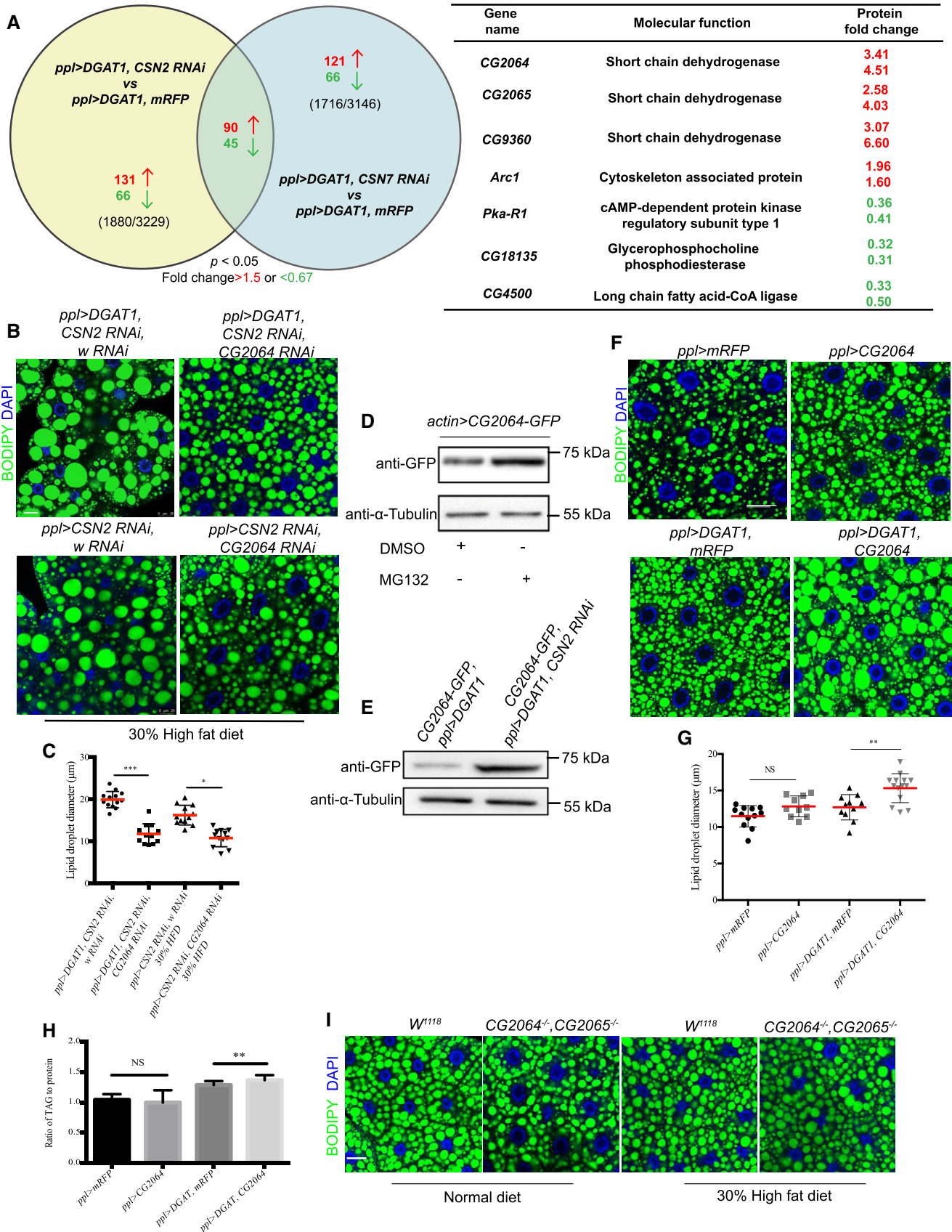


Figure 2.

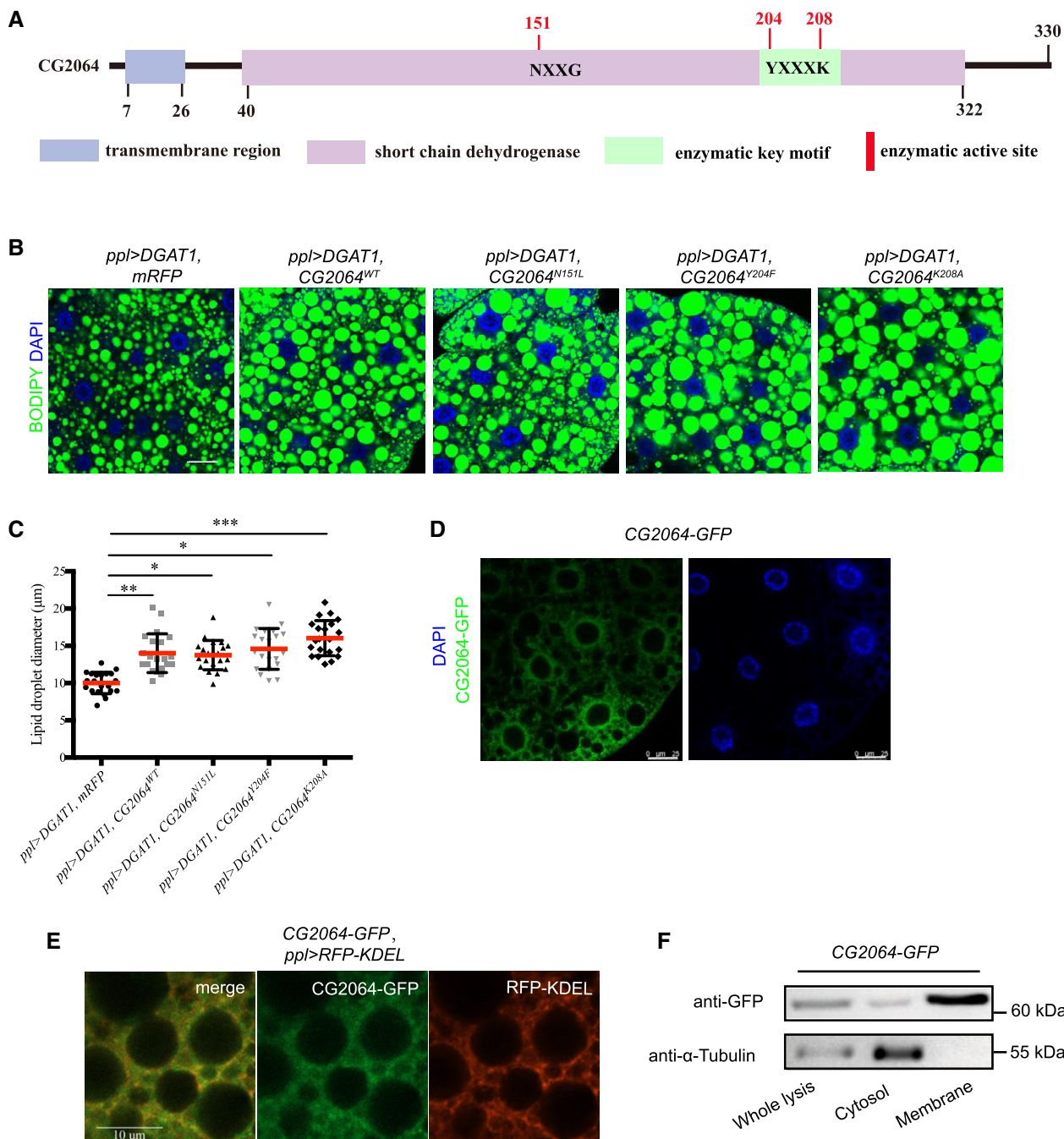


Figure 3. The membrane protein RDH/CG2064 regulates lipid droplet size independent of its enzymatic activity.

A The protein domain structure of RDH/CG2064. Grey box: predicted transmembrane region; Pink box: short-chain dehydrogenase domain. The key enzymatic motif (YXXXK) and active site (NXXG) are shown.

B 3rd instar larval fat bodies were stained by BODIPY (green) for lipid droplets and DAPI (blue) for nuclei. Overexpressing wild-type or site-mutated *RDH/CG2064* increases the lipid droplet size in larvae with *DGAT1* overexpression (*ppl>DGAT1*). Scale bar represents 25 μm.

C Quantification of the lipid droplet size in (B).

D Immunofluorescent staining of RDH/CG2064-GFP with anti-GFP antibody in 3rd instar larval fat body. DAPI (blue) stains nuclei. RDH/CG2064 is enriched in the perinuclear region. Scale bar represents 25 μm.

E Immunofluorescence imaging of RDH/CG2064-GFP, detected with anti-GFP antibody, and the ER protein marker RFP-KDEL in 3rd instar larval fat body. RDH/CG2064 co-localizes with RFP-KDEL. Scale bar represents 10 μm.

F Whole lysates and cytosolic and membranous fractions were prepared from fat body samples of 3rd instar larvae expressing an *RDH/CG2064-GFP* knockin reporter. RDH/CG2064-GFP protein was detected by anti-GFP antibody in a western blot. RDH/CG2064-GFP is mainly present in the membranous fraction.

Source data are available online for this figure.

size. In 3rd instar larval fat body, RDH/CG2064 overexpression did not change the lipid droplet size under normal conditions, but it led to large lipid droplets with *DGAT1* OE (Figs 2F and G, and EV2C and D). TAG measurement yielded a similar result (Fig 2H). In addition, in animals fed on a high-fat diet, *DGAT1* RNAi suppressed the large lipid droplet phenotype induced by *RDH/CG2064* OE (Fig EV3B). This suggests that RDH/CG2064 is likely a main target of CSN in regulating lipid droplet size under high-fat conditions.

We also examined the phenotype of *RDH/CG2064* RNAi and mutants. The RNAi efficiency was verified by Q-RT-PCR (Fig EV3C). In addition, the protein level of RDH/CG2064-GFP was reduced upon *RDH/CG2064* knockdown (Fig EV3D). We found that knockdown of *RDH/CG2064* did not change the lipid droplet size in the fat body of wild-type and *DGAT1* OE 3rd instar larvae (Fig EV3E). Considering that *RDH/CG2064* and *CG2065* are neighboring genes and both RDH/CG2064 and *CG2065* levels are increased in *CSN2/CSN7* RNAi, we generated *RDH/CG2064* and *CG2065* double deletion mutants to further examine the loss-of-function phenotype. We found that the lipid droplet size was not dramatically changed in the double mutants compared with controls under normal diet or high-fat diet conditions (Fig 2I). This suggests that *RDH/CG2064* is not required to maintain lipid droplet size under normal conditions.

RDH/CG2064 regulates lipid droplet size independent of its enzymatic activity

We next investigated the mechanism by which RDH/CG2064 regulates lipid droplet size. RDH/CG2064 has a transmembrane (TM) domain at its N-terminus followed by a large dehydrogenase/reductase domain (Fig 3A). By BLAST, RDH/CG2064 is close to the mammalian RDH11/12 family. RDH12 is localized on the ER and its activity modulates retinol homeostasis (Keller & Adamski, 2007). ENV9, the yeast homolog of RDH12, increases lipid droplet size in a reductase activity-dependent manner (Siddiqah et al, 2017). Therefore, we first examined whether the enzymatic activity of RDH/CG2064 is required for lipid droplet size regulation. The SDR proteins have a YXXXK motif, which is the reductase catalytic sequence (Jornvall et al, 1995). We generated two mutations in the enzymatic domain YXXXK motif, Y204F and K208A, and an upstream active site mutation, N151L (Fig 3A). Surprisingly, overexpressing these putative reductase-dead forms of RDH/CG2064 also increased the lipid droplet size in the fat body of 3rd instar *DGAT1*

OE larvae (Fig 3B and C), which suggests that RDH/CG2064 regulates lipid droplet size independent of its enzymatic activity.

We then examined the sub-cellular location of RDH/CG2064 with the help of the RDH/CG2064-GFP knockin reporter. The fluorescent signal of RDH/CG2064-GFP in 3rd instar larval fat body is very weak, so we boosted the signal by anti-GFP antibody staining. RDH/CG2064-GFP is not enriched on lipid droplets. Instead, the signal is smeared and enriched around the nucleus, likely reflecting the perinuclear ER region (Fig 3D). We further examined the sub-cellular location of RDH/CG2064-GFP by co-labeling with the ER protein marker RFP-KDEL. High-resolution confocal microscopy revealed strong co-localization between the RDH/CG2064-GFP signal and the ER marker signal (Fig 3E). To further examine the distribution of RDH/CG2064-GFP, we separated whole lysates of 3rd instar larval fat body into cytosolic and membranous fractions through super-speed centrifugation. By western blot analysis, the majority of the RDH/CG2064-GFP was found in the membranous fraction (Fig 3F), further supporting the ER localization of RDH/CG2064-GFP.

RDH/CG2064 interacts with the lipid droplet protein Plin2

To reveal the molecular mechanism by which RDH/CG2064 regulates lipid droplet size, we next used anti-GFP antibody and performed immunoprecipitation-mass spectrometry (IP-MS) of RDH/CG2064-GFP with GFP as control to identify the interacting protein partners of RDH/CG2064. Among the potential RDH/CG2064-interacting proteins, the lipid droplet-associated Perilipin protein Plin2 is the most obvious candidate (Table EV1). *Drosophila* has two Perilipin proteins, Plin1 and Plin2 (Blanchette-Mackie et al, 1995; Miura et al, 2002; Welte et al, 2005). *Plin2* genetically antagonizes *brummer* lipase (*bmm*), the sole *Drosophila* homolog of ATGL lipase (Zimmermann et al, 2004; Gronke et al, 2005), and overexpression of *Plin2* increases lipid droplet size (Gronke et al, 2003; Bi et al, 2012). To validate the interaction of RDH/CG2064 and Plin2, we expressed a N-terminal Flag-tagged RDH/CG2064 in Plin1-GFP, Plin2-GFP, or Bmm-GFP functional knockin *Drosophila* reporter lines. Immunoprecipitations with anti-Flag antibody show that RDH/CG2064 pulls down Plin2, but not Plin1 or Bmm (Fig 4A). Furthermore, the physical interaction of RDH/CG2064 and Plin2 is also robust when *DGAT1* is overexpressed (Fig 4B).

We investigated the interaction of RDH/CG2064 and Plin2 further. RDH/CG2064 contains a TM domain and a dehydrogenase/

Figure 4. RDH/CG2064 interacts with Plin2.

- A, B Lysates of 3rd instar larval fat body samples of different genetic backgrounds were immunoprecipitated with anti-Flag antibody and then probed by anti-GFP or anti-Flag antibody in a western blot. Plin2, but not Plin1 or Bmm, is specifically coimmunoprecipitated with RDH/CG2064 (A). Plin2 was coimmunoprecipitated with RDH/CG2064 in samples from larvae overexpressing *DGAT1* (B).
- C Schematic diagram of full-length RDH/CG2064 and TM domain-deleted RDH/CG2064 (Δ TM). Lysates of *Drosophila* S2 cells expressing the different proteins were immunoprecipitated with anti-GFP antibody and detected by anti-GFP or anti-Flag antibody in a western blot. Both full-length and Δ TM RDH/CG2064 were coimmunoprecipitated with Plin2.
- D Schematic diagram of Plin1, Plin2, and the Plin2-Plin1-C chimeric protein. Lysates of *Drosophila* S2 cells expressing the different proteins were immunoprecipitated with anti-Flag antibody and then probed by anti-GFP or anti-Flag antibody in a western blot. Neither Plin1 nor Plin2-Plin1-C chimeric protein coimmunoprecipitated with RDH/CG2064.
- E Lysates of *Drosophila* S2 cells expressing full-length Plin1 or Plin1 with a C-terminal deletion (Plin1 Δ C) were immunoprecipitated with anti-Flag antibody and then probed by anti-GFP or anti-Flag antibody in a western blot. Plin1 Δ C coimmunoprecipitated with RDH/CG2064.
- F 3rd instar larval fat bodies were stained by BODIPY (green) for lipid droplets and DAPI (blue) for nuclei. Under high-fat conditions, *RDH/CG2064* overexpression increases the lipid droplet size, and *Plin2* RNAi suppresses the enlargement induced by *RDH/CG2064* overexpression. Scale bar represents 25 μ m.

Source data are available online for this figure.

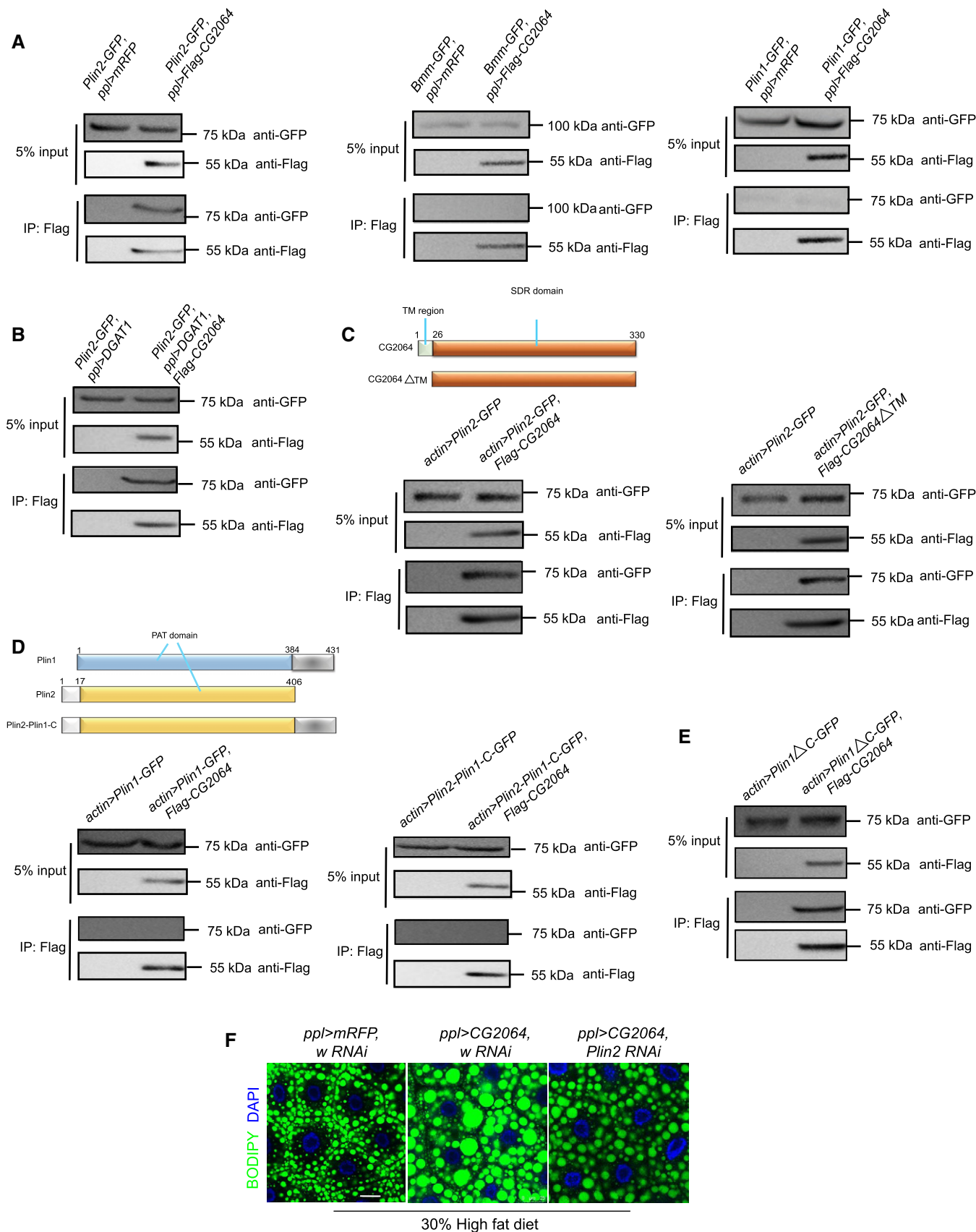


Figure 4.

reductase domain (Fig 3A). We expressed Plin2-GFP with Flag-tagged full-length RDH/CG2064 or TM domain-deleted RDH/CG2064 in *Drosophila* S2 cells. Both versions of RDH/CG2064 interact with Plin2 when immunoprecipitated with anti-GFP antibody, indicating that the TM domain of RDH/CG2064 is not required for its interaction with Plin2 (Fig 4C). Plin1, the other *Drosophila* PAT domain protein, has an extended C-terminal region compared with Plin2 (Fig 4D). Previous study showed that this C-terminal region is essential for the sub-cellular location of Plin1 and determines the functional difference between Plin1 and Plin2 (Bi et al, 2012). Considering that Plin2, but not Plin1, is able to interact with RDH/CG2064, we hypothesized that the C-terminal region of Plin1 may prevent its interaction with RDH/CG2064. Therefore, we expressed a chimeric Plin2-Plin1-C-terminal fusion protein along with Flag-tagged RDH/CG2064 in S2 cells. This fusion protein does not bind to RDH/CG2064 when immunoprecipitated with anti-Flag antibody (Fig 4D). Furthermore, although full-length Plin1 does not interact with RDH/CG2064, Plin1 with a C-terminal deletion does indeed interact with RDH/CG2064 (Fig 4E). Together, these results show that RDH/CG2064 interacts with Plin2, but not Plin1, and the C-terminal region of Plin1 may prevent its association with RDH/CG2064. Moreover, genetic analysis results suggest that Plin2 acts downstream of RDH/CG2064. The large lipid droplet phenotype of *RDH/CG2064* OE animals on a high-fat diet is suppressed upon *Plin2* knockdown (Fig 4F).

RDH/CG2064 changes the sub-cellular localization of Plin2

Next, we investigated whether the CSN-RDH/CG2064 axis affects Plin2. We first examined the protein level of Plin2-GFP by western blot. In fat body samples from 3rd instar *DGAT1* OE larvae with *ppl>CSN2* RNAi or *ppl>RDH/CG2064* overexpression, there is no evident difference in Plin2-GFP level compared with the *DGAT1* OE control (Fig EV3F). This suggests that the CSN-RDH/CG2064 axis does not affect the Plin2 protein level.

We then explored whether RDH/CG2064 affects the subcellular localization of Plin2. Previous protein overexpression studies show that Plin2 is usually found in small lipid droplets, in particular lipid droplets in the cortical region of larval fat cells (Bi et al, 2012), which are also called peripheral lipid droplets (Diaconeasa et al, 2013). Consistent with previous overexpression results, the Plin2-GFP signal from the endogenous knockin reporter is also prone to localize on

small cortical lipid droplets close to the plasma membrane in wild-type 3rd instar larval fat body. In *CSN2* RNAi or *RDH/CG2064* overexpression conditions, the peripheral Plin2-GFP signal is greatly reduced and the GFP signal is increased in medial lipid droplets (Fig 5A and B). In addition, the localization of Plin2 is significantly increased on lipid droplets around the nucleus (Fig 5A and B). This finding is in line with the peri-nuclear ER localization of RDH/CG2064. Therefore, although elevated expression of RDH/CG2064 in wild type is not sufficient to form large lipid droplets, it promotes the localization of more Plin2 to peri-nuclear and medial lipid droplets. Such a localization change may prime the lipid droplets so that they are ready to expand.

We further investigated the effect of the CSN-RDH/CG2064 axis on Plin2 localization under high-fat conditions. The peripheral Plin2 localization is reduced in the fat body of 3rd instar *DGAT1* OE larvae with *CSN2* RNAi or *RDH/CG2064* overexpression (Fig 5C–E). In these animals, more Plin2-GFP signal is present in large medial lipid droplets (Fig 5C–E). Similar changes of Plin2 localization were also observed in 3rd instar larval fat body of *CSN2* RNAi animals reared on 30% high-fat medium (Fig 5F). Together, these results demonstrate that elevation of RDH/CG2064 level promotes the localization of Plin2 to medial lipid droplets and lipid droplets around the nucleus.

Peripheral Plin2 is important for the maintenance of small cortical lipid droplets (Ugrankar et al, 2019). In line with the reduction of peripheral Plin2, the number of small peripheral lipid droplets is greatly reduced in the fat body of 3rd instar larvae with *CSN* RNAi or *RDH/CG2064* overexpression in both control and *DGAT1* OE conditions (Fig 5G; Movies EV1 and EV2). This phenotype is more severe in *CSN3* RNAi fat body than in *RDH/CG2064* fat body. It is possible that *RDH/CG2064* may be a major downstream target of CSN, but not the only one. Taking the peri-nuclear enrichment of RDH/CG2064 into account, these results suggest that the increased level of RDH/CG2064 results in the localization of more Plin2 to lipid droplets around the nucleus. These may represent newly formed lipid droplets from the peri-nuclear ER and they may grow into large lipid droplets under high-fat conditions.

The RDH/CG2064-Plin2 axis reduces the level of Bmm lipase

We further explored the consequence of RDH/CG2064-mediated changes in Plin2 localization. Genetic analysis revealed that Plin2 antagonizes the activity of Bmm (Gronke et al, 2005). Our previous

Figure 5. The CSN-RDH/CG2064 axis changes the sub-cellular localization of Plin2.

Images of Plin2-GFP in 3rd instar larval fat body cells of different genotypes. Scale bar represents 25 μ m.

- CSN2* RNAi or *RDH/CG2064* overexpression reduces the peripheral localization of Plin2-GFP and increases the localization of Plin2-GFP on small peri-nuclear lipid droplets (boxed). DAPI (blue) stains nuclei. White arrows indicate peripheral lipid droplet. Red arrows indicate medial lipid droplets.
- The peripheral localization of Plin2-GFP is greatly reduced in fat body cells from larvae with *CSN2* RNAi or *RDH/CG2064* overexpression. Images were taken by focusing on the periphery of fat cells.
- In fat body cells from *ppl>DGAT1* larvae with *CSN2* RNAi or *RDH/CG2064* overexpression, the localization of Plin2-GFP is greatly reduced at the periphery and is dramatically increased on large medial lipid droplets. White arrows indicate peripheral lipid droplet. Red arrows indicate medial lipid droplets.
- Fluorescence intensity line plots of the images in (C). GFP intensity along the line across a lipid droplet was measured by ImageJ. In *ppl>DGAT1* larvae with *CSN2* RNAi or *RDH/CG2064* overexpression, Plin2-GFP localization on large medial lipid droplets is represented by two peaks. More than 30 lipid droplets were measured for each genotype. The plot shown is a typical image curve for the indicated genotype.
- The peripheral localization of Plin2-GFP is greatly reduced in fat body cells from *ppl>DGAT1* larvae with *CSN2* RNAi or *RDH/CG2064* overexpression. Images were taken by focusing on the periphery of fat cells.
- The localization of Plin2-GFP is greatly reduced in peripheral lipid droplets and increased in medial lipid droplets in *CSN2* RNAi larvae fed on a 30% high-fat diet. DAPI (blue) stains nuclei. White arrows indicate peripheral lipid droplet. Red arrows indicate medial lipid droplets.
- The peripheral lipid droplets in larval fat body cells from different genetic backgrounds were stained by BODIPY (green). *CSN3* RNAi or *RDH/CG2064* overexpression reduces the number of peripheral lipid droplets in both wild-type and *ppl>DGAT1* larvae.

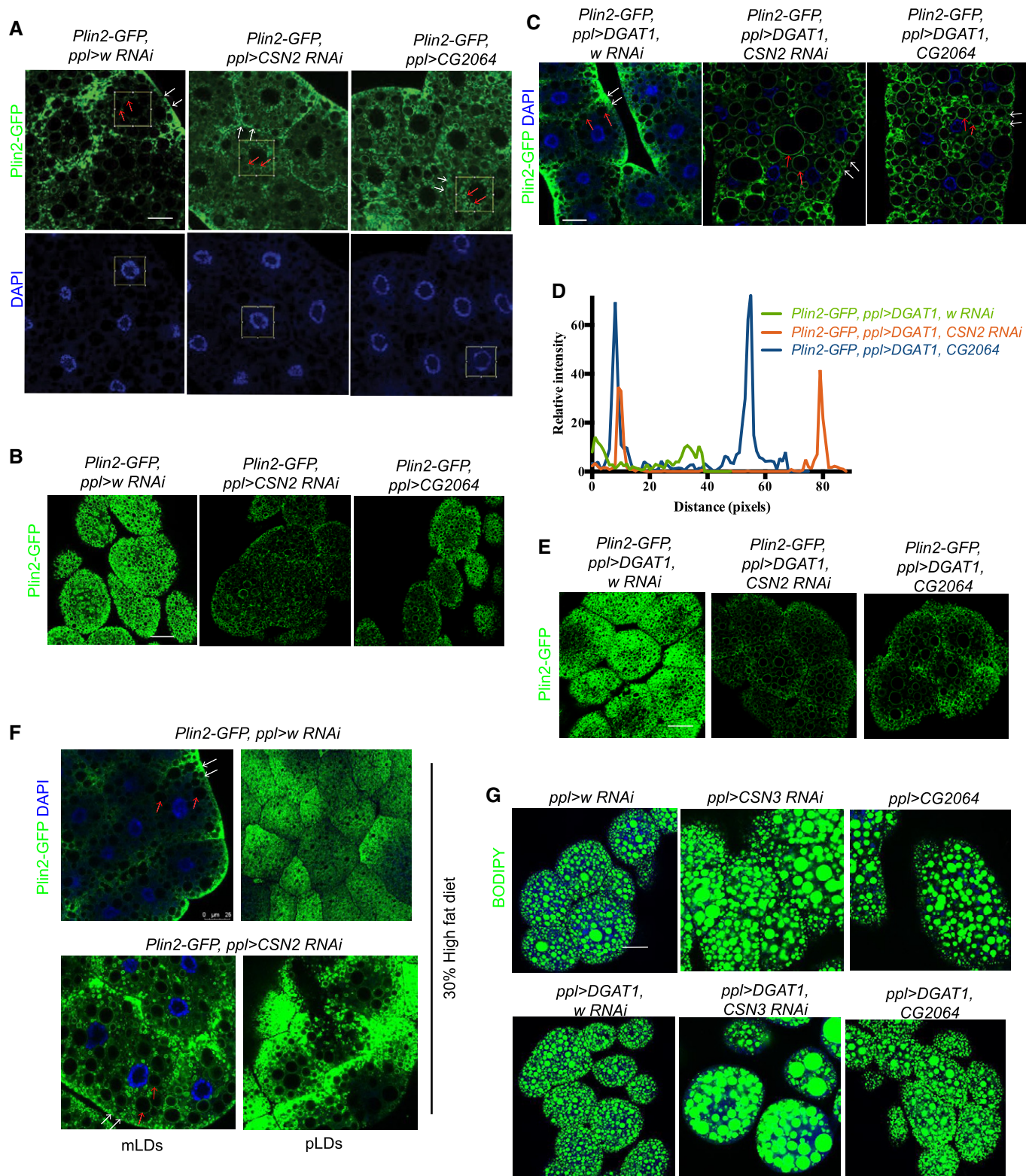


Figure 5.

study also suggested that “Plin2 may protect small lipid droplets at an early stage of lipid droplet biogenesis from Bmm-mediated lipolysis” (Bi *et al.*, 2012). Therefore, it is possible that the RDH/CG2064-Plin2 axis affects Bmm.

We examined the cellular location of Bmm lipase with the help of a functional Bmm-GFP knockin reporter. In the *ppl>DGAT1* over-expression control, the fluorescent signal of Bmm-GFP was found in the cytosol and also exhibited a punctate pattern surrounding lipid

droplets in 3rd instar larval fat body (Fig 6A and B). Interestingly, the GFP signal was greatly diminished and the peri-lipid droplet punctate localization was absent in the fat body of 3rd instar *DGAT1* OE larvae with *CSN2* RNAi or *RDH/CG2064* overexpression (Fig 6A and B). The reduction of Bmm-GFP fluorescent signal was also confirmed by western blot (Fig 6C). Furthermore, the reduction of overall Bmm-GFP fluorescent signal and peri-lipid droplet localization of Bmm-GFP was similarly found in 3rd instar fat body of *CSN2* RNAi larvae fed on a 30% high-fat diet (Fig 6D).

We also examined the localization of Bmm-GFP in *DGAT1* OE larvae with *Plin2* overexpression. The localization of Bmm-GFP is not changed in the fat body of 3rd instar larvae overexpressing *DGAT1* alone (Fig 6E). In contrast, the lipid droplet-localized Bmm-GFP in 3rd instar *DGAT1* OE larval fat body is dramatically reduced when *Plin2* is also overexpressed (Fig 6F and G). This phenotype is very similar to that of *RDH/CG2064* overexpression (Fig 6A and B). Therefore, the *RDH/CG2064-Plin2* axis likely reduces the level and the peri-lipid droplet localization of Bmm under high-fat conditions.

If a reduced level of Bmm lipase lies downstream of the *RDH/CG2064-Plin2* axis, knocking down *bmm* should increase the lipid droplet size when *DGAT1* is overexpressed. Previous studies show that *bmm* mutants exhibit an early onset obese phenotype in adulthood, but not at the larval stage (Gronke et al, 2005, 2007; Bi et al, 2012). Consistent with that, lipid droplets were not enlarged in the fat body of 3rd instar larvae with *bmm* RNAi (Fig 6H and I). In contrast, lipid droplet size was significantly increased in the fat body of 3rd instar *DGAT1* OE larvae with *bmm* RNAi (Fig 6H and I). TAG measurement yielded a similar result (Fig 6J).

To follow the kinetics of CSN-mediated *RDH/CG2064* degradation and changes in the Bmm protein level, we turned to *Drosophila* S2 cultured cells. We treated cells expressing *RDH/CG2064-GFP* or Bmm-GFP with cycloheximide (CHX), a protein synthesis inhibitor. In control cells, the level of *RDH/CG2064-GFP* protein started to decline within 1 h of CHX treatment, and no *RDH/CG2064-GFP* protein was detected after 6-h CHX treatment. In *CSN5* RNAi cells, the *RDH/CG2064-GFP* signal persisted longer than in control cells

(Fig 7A and B). For Bmm-GFP, the protein level started to decline within 1–2 h after CHX treatment in control cells. In *CSN5* RNAi cells, the Bmm-GFP level declined faster than in control cells (Fig 7C and D). These data are consistent with the findings in larval fat cells. Together, these results support the idea that the *RDH/CG2064-Plin2* axis reduces the level of Bmm lipase.

The CSN-RDH-Plin2 axis is not affected by high-fat feeding and is required for survival under prolonged starvation

The lipid droplet phenotype of *CSN* RNAi is only observed in animals fed on a high-fat diet. This raises the possibility that CSN tunes down *RDH/CG2064-Plin2* under high-fat conditions. Therefore, we compared the levels of *RDH/CG2064*, *Plin2*, and Bmm under normal and high-fat conditions using GFP knockin reporters. There was no difference in the levels of *RDH/CG2064-GFP*, *Plin2-GFP*, and Bmm-GFP under normal and high-fat conditions (Fig EV4A–C), which suggests that the *CSN-RDH/CG2064-Plin2* axis is not affected by high-fat feeding. *RDH/CG2064-GFP* remains localized in the ER under high-fat conditions (Fig EV4D). Indeed, similar to high-fat conditions (Fig 2E), both *CSN2* RNAi and *CSN7* RNAi dramatically increase the level of *RDH/CG2064-GFP* under normal conditions (Fig 7E). These results, together with the regulatory effect of CSN on *RDH/CG2064* and Bmm levels in S2 cells, suggest that CSN regulates the turnover of *RDH/CG2064* under both normal and high-fat conditions.

The previous results raise the possibility that the *CSN* RNAi phenotype is subtle under normal conditions and can only be revealed under certain sensitizing conditions. Under starvation, lipolysis mobilizes lipids from fat cells to support animal survival and also promotes the formation of lipid droplets in oenocytes, hepatocyte-like cells in *Drosophila*. We therefore assayed the impact of *CSN* RNAi on both oenocyte lipid storage and larval survival under starvation. After 6 h of starvation, there is no obvious difference in lipid storage in oenocytes of *CSN2* RNAi and *CSN7* RNAi compared with control under both normal and high-fat conditions

Figure 6. The CSN-RDH/CG2064-Plin2 axis affects the level and lipid droplet localization of Bmm lipase.

Confocal images of Bmm-GFP (green) in 3rd instar larval fat bodies of different genotypes. DAPI (blue) stains nuclei. Scale bar represents 25 μ m.

- A Knocking down *CSN2* or overexpressing *RDH/CG2064* in animals with *DGAT1* overexpression (*ppl>DGAT1*) decreases the level and lipid droplet localization of Bmm-GFP.
- B The GFP intensity along the line across a lipid droplet in (A) was measured by ImageJ. The lipid droplet localization of Bmm-GFP, represented by two peaks, is clearly visible in fat cells from *ppl>DGAT1* larvae, but it is lost in fat cells from *ppl>DGAT1* larvae with *CSN2* RNAi or overexpression of *RDH/CG2064*. More than 30 lipid droplets of each genotype were measured. One typical image curve is shown for each genotype.
- C The level of Bmm-GFP in 3rd instar larval fat bodies of different genotypes was detected by anti-GFP antibody in a western blot. In *ppl>DGAT1* larvae, *CSN2* RNAi or overexpression of *RDH/CG2064* decreases the level of Bmm.
- D *CSN2* RNAi decreases the level and lipid droplet localization of Bmm-GFP in fat cells from larvae fed on a 30% high-fat diet.
- E The level and lipid droplet localization of Bmm-GFP are similar in fat cells from larvae overexpressing *DGAT1* or mRFP (control).
- F Overexpression of *Plin2* decreases the level and lipid droplet localization of Bmm-GFP in fat cells from larvae with *DGAT1* overexpression.
- G GFP intensity along the line across a lipid droplet from (F) was measured by ImageJ. The lipid droplet localization of Bmm-GFP, represented by two peaks, was evident in fat cells from *ppl>DGAT1* larvae, but is lost in *ppl>DGAT1* larvae with overexpression of *Plin2*. More than 30 lipid droplets of each genotype were measured. One typical image curve is shown for each genotype.
- H 3rd instar larval fat bodies were stained by BODIPY (green) for lipid droplets and DAPI (blue) for nuclei. *bmm* RNAi increases the lipid droplet size in fat cells from larvae with *DGAT1* overexpression. Scale bar represents 25 μ m.
- I Quantification of the lipid droplet size in (H). Data were analyzed by one-way ANOVA with a *post hoc* Turkey's multiple-comparison test. Each point represents data from one fat body. At least 30 cells were analyzed from each fat body. Error bars represent \pm SEM. ****P* < 0.001 and NS: non-significant.
- J Relative TAG levels in different genetic backgrounds were measured by glyceride assay kit. For quantification, TAG levels were normalized to protein. Error bars represent \pm SEM. ***P* < 0.01 and ****P* < 0.001.

Source data are available online for this figure.

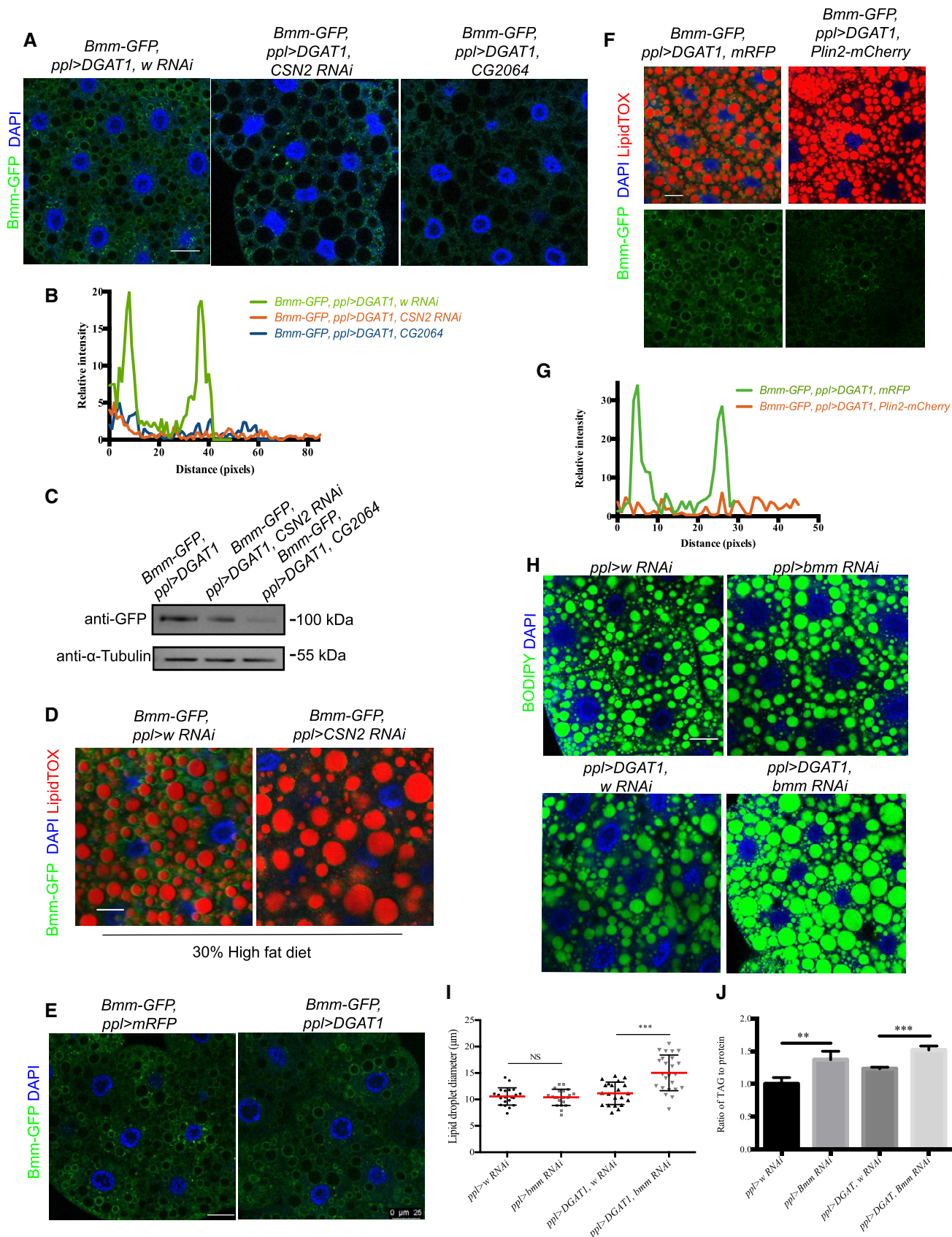


Figure 6.

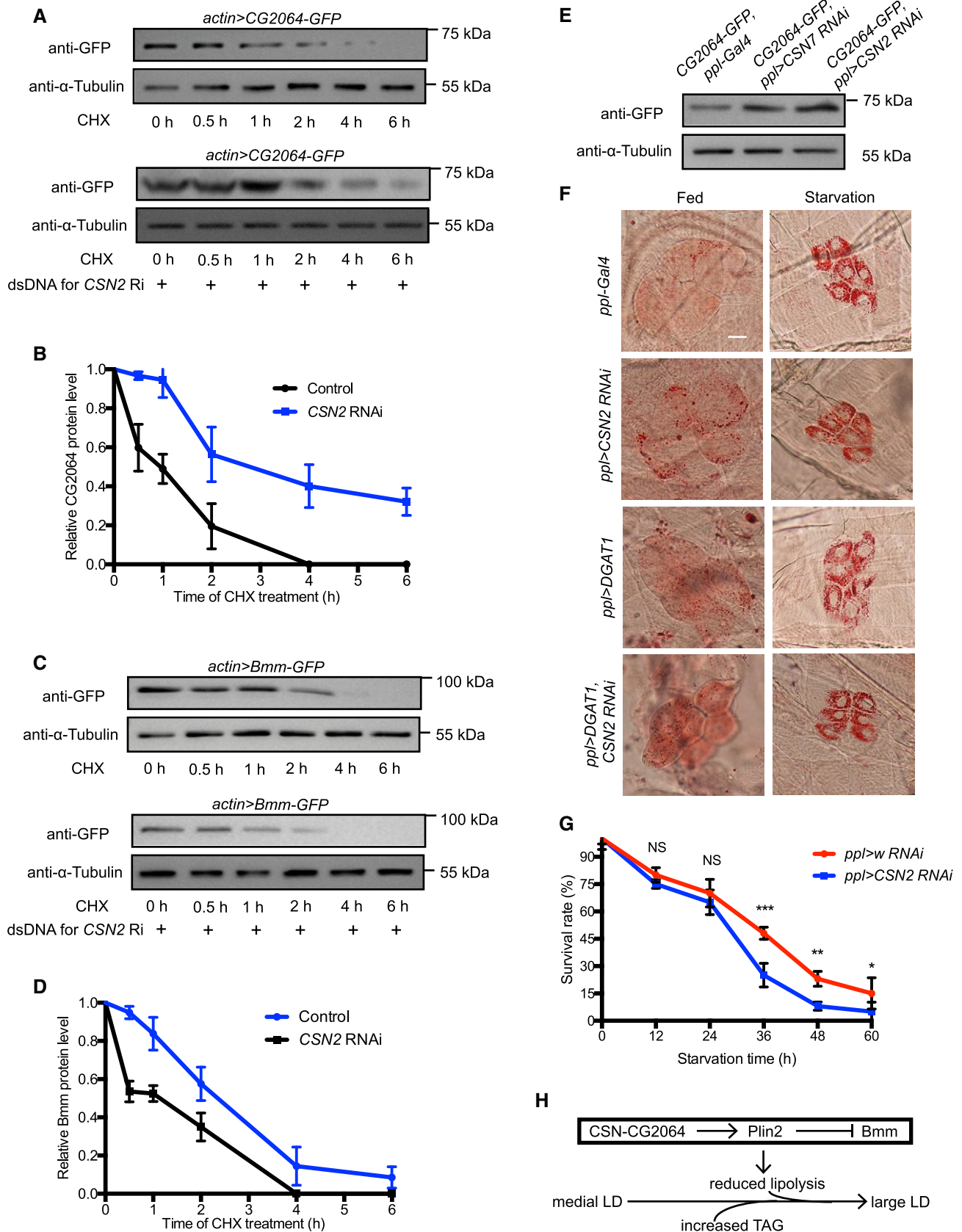


Figure 7.

Figure 7. The CSN-RDH-Plin2 axis functions under normal conditions and is required for prolonged starvation.

- A S2 cells expressing RDH/CH2064-GFP were treated with the protein synthesis inhibitor cycloheximide (CHX) for the indicated time (h: hours). The level of RDH/CH2064-GFP was determined by western blotting using anti-GFP antibody. Tubulin was used as loading control.
- B Quantification of the relative RDH/CH2064-GFP protein levels in (A). Error bars represent \pm SEM.
- C S2 cells expressing Bmm-GFP were treated with the protein synthesis inhibitor cycloheximide (CHX) for the indicated time (h: hours). The level of Bmm-GFP was determined by western blotting using anti-GFP antibody. Tubulin was used as loading control.
- D Quantification of the relative Bmm-GFP protein levels in (C). Error bars represent \pm SEM.
- E The RDH/CG2064-GFP protein level in 3rd instar larval fat cells is increased in CSN2 or CSN7 RNAi, as detected by anti-GFP antibody in a western blot. Tubulin was used as loading control.
- F Oil red staining of 3rd instar larval oenocytes in different genetic backgrounds under fed or starvation conditions.
- G The survival rate of control and CSN2 RNAi larvae at various fasting time points. Error bars represent \pm SEM. * P < 0.05; ** P < 0.01; *** P < 0.001; and NS: non-significant.
- H Schematic model showing how the CSN-RDH/CG2064-Plin2 axis inhibits Bmm and promotes the formation of large lipid droplets under high-fat/increased TAG conditions.

Source data are available online for this figure.

(Fig 7F). In addition, there is no significant difference in the larval survival rate in control and CSN2 RNAi animals up to 24 h of starvation (Fig 7). However, the CSN2 RNAi larvae exhibited a much lower survival rate at 36–60 h of fasting compared with controls (Fig 7G). This suggests that the CSN-RDH-Plin2 axis is likely required for larval survival under prolonged starvation.

Discussion

The size and the associated proteins of lipid droplets vary greatly in cells. Here, we discover that the CSN complex prevents the enlargement of lipid droplets under high-fat conditions. CSN controls the proteasomal degradation of RDH/CG2064, which interacts with Plin2. The elevated level of RDH/CG2064 in CSN knockdown larvae changes Plin2 localization from peripheral lipid droplets to medial lipid droplets and small lipid droplets around the nucleus. Plin2 likely protects these lipid droplets from lipolysis by reducing the level of Bmm/ATGL lipase and facilitates the formation of large lipid droplets under lipid-overload conditions (Fig 7H).

Different CSN subunits and Cullin4 have been identified in previous studies for genes that affect lipid droplet morphology and lipid storage (Guo *et al*, 2008; Baumbach *et al*, 2014; Yoshizawa *et al*, 2014; Sinha *et al*, 2020). Although the targets of CSN-Cul4 in regulating lipid storage have not been previously reported, these studies, together with our findings here, clearly support the important role of CSN-CUL4 in both cellular and organismal lipid storage. We further identified RDH/CG2064 as a target of CSN-Cul4 in regulating lipid droplet size. RDH/CG2064 is a member of SDR, a large enzyme superfamily mainly defined by a similar three-dimensional structure and catalytic amino acid tetrad. RDH and HSD, two SDR subfamilies, have been linked to lipid droplets or lipid storage-related diseases (Sandell *et al*, 2007; Deisenroth *et al*, 2011; Jiang & Napoli, 2013; Su *et al*, 2014; Siddiqah *et al*, 2017). Some of these proteins are localized on lipid droplets and regulate lipid droplet dynamics in either an enzymatic activity-dependent or -independent manner. RDH/CG2064 is closely related to the RDH11 and RDH12 subfamily. Similar to RDH12, RDH/CG2064 is likely localized in the ER. RDH12 takes part in retinoid/vitamin A production. Retinoid is reported to be negatively associated with the content of body fat in mammals (Berry & Noy, 2009). *RDH11* mutation causes retinitis pigmentosa in humans (Xie *et al*, 2014). Besides the retina, murine RDH11 is also

expressed in the liver and acts as an all-*trans*-retinaldehyde reductase to maintain the level of all-*trans*-retinol under reduced vitamin A availability (Belyaeva *et al*, 2018). Previous studies mainly focused on its role in retinol metabolism and it is not known whether RDH11 regulates neutral lipid storage. Our findings raise the possibility that RDH11 may have dual functions, one in lipid droplet dynamics and the other in retinoid metabolism. Further studies are required to dissect the role of RDH11 in lipid metabolism and retinitis pigmentosa.

RDH/CG2064 regulates lipid droplet size through Plin2. RDH/CG2064 is localized on the ER, so how does it affect the localization of the lipid droplet protein Plin2 from peripheral lipid droplets to perinuclear and medial lipid droplets? It is possible that through direct binding, RDH/CG2064 retains Plin2 in the perinuclear ER region, where the biogenesis of medial lipid droplets mainly occurs. A higher level of Plin2 facilitates the expansion of newly formed lipid droplets. The growth of medial lipid droplets is affected by both *de novo* lipogenesis and high-fat feeding. In combination with high-fat conditions, the increased level of Plin2 in medial lipid droplets and lipid droplets around the nucleus likely results in the appearance of large lipid droplets (Fig EV4E). Consistent with this, when the level of RDH/CG2064 is elevated, the size of peripheral lipid droplets is reduced, while the size of medial lipid droplets is increased.

PLINs reside in the hub for regulating lipid droplet dynamics, including lipolysis and lipid droplet fusion (Beller *et al*, 2010; Sun *et al*, 2013; Kimmel & Sztalryd, 2016). Previous studies show that different PLINs act as either activity regulators or protein localization barriers of lipolysis, in particular for the rate-limiting lipase ATGL (Zimmermann *et al*, 2004; Listenberger *et al*, 2007). Although numerous downstream effectors of PLINs have been identified (Granneman *et al*, 2009; Sun *et al*, 2013), the upstream regulators of PLINs are relatively less well characterized. The best known one is protein kinase A (PKA), which phosphorylates PLIN1. The RDH/CG2064-Plin2-Bmm/ATGL axis is somewhat different from the PKA-PLIN1-ATGL axis. The phosphorylation of PLIN1 by PKA changes the binding partner of PLIN1 and then results in ATGL activation. The binding of RDH/CG2064 with PLIN2 changes the localization of PLIN2 and likely reduces the lipid droplet localization and the level of Bmm/ATGL. These two axes may represent two layers of ATGL activity regulation. One aims for full activation and the other limits initial basal activation. The RDH/CG2064-Plin2-Bmm/ATGL axis

may determine the level of ATGL that is in the initial “ready-to-go” state. Full activation of ATGL then occurs by its interaction with the coactivator CGI-58, which is unleashed via the PKA-PLIN1-ATGL axis. The coordination of these two pathways may be helpful for correct spatial or temporal ATGL activation in different types of lipid droplets.

CSN and RDH/CG2064 represent a new type of lipid droplet regulator that is usually not required under normal physiological conditions and thus cannot be easily identified. Such regulators may be poorly characterized or even missed in previous functional studies. However, with the current pandemic of obesity, they may hold great potential for understanding or treating lipid-overload diseases. Further functional and clinical studies on this type of regulator may shed more light on systemic lipid homeostasis.

Materials and Methods

Drosophila husbandry and stocks

Unless specified, flies were raised on standard cornmeal food (8 g agar, 63.2 g glucose, 31.6 g sucrose, 30 g yeast, 77.7 g corn powder, butylparaben into 1 l water) at 25°C. The high-fat diet contains 30% coconut oil in cornmeal food. *ppl-GAL4* was used to drive gene overexpression or knockdown in the fat body (Liu et al, 2014). For the RNAi screen, a collection of *ppl-GAL4>DGAT1* virgin flies were crossed to *UAS-RNAi* males. The eggs were raised at 25°C, then transferred to 29°C at 48 h after egg laying. For RNAi, *UAS-white RNAi* was chosen as the control RNAi group, while for overexpression, *UAS-mRFP* (membrane myr-RFP) was used as the UAS control. Transgenes of *pUAST-Flag-CG2064*, *pUAST-CG2064-GFP*, *pUAST-CG2064^{N151L}*, *pUAST-CG2064^{K208A}*, and *pUAST-CG2064^{Y204F}* were generated. *Plin1-GFP*, *Plin2-GFP*, *Bmm-GFP*, and *CG2064-GFP* knockin flies were generated by the CRISPR/Cas9 technique. *Plin1/CG10374* has four transcripts, which share the same C-terminal region. We designed guide RNAs which target the shared C-terminal region. Using CRISPR/Cas9, the endogenous *Plin1* C-terminal was replaced by a donor sequence which was fused in frame with GFP. *Plin2/CG9057* has five transcripts, which share the same C-terminal region. *Bmm/CG5295* has two transcripts, which share the same C-terminal region. *CG2064-GFP* has only one transcript. Based on a similar approach to *Plin1-GFP*, we generated *Plin2* C-terminal GFP, *Bmm* C-terminal GFP, and *CG2064* C-terminal GFP knock-in flies. Other *Drosophila* stocks were obtained from Bloomington *Drosophila* Stock Center and Tsinghua Fly Center. Fly lines used in this study are listed (Table EV2).

Tissue staining, microscopy, and image analysis

Fat bodies of wandering 3rd instar larvae were dissected in 1x PBS buffer. The dissected samples were fixed with 4% paraformaldehyde for 30 min at room temperature. To stain lipid droplets, fixed fat bodies were incubated for 1 h at room temperature in the neutral lipid dye BODIPY 493/503 (Invitrogen, 1 mg/ml diluted 1:500 with PBS). The washed samples were incubated with 2 ng/μl DAPI to label the nuclei. The images were taken in the middle plane of the fat body cells, where the nucleus is largest, to estimate lipid droplet size according to the same criterion. To quantify the lipid droplet

size, the diameters of the top three largest lipid droplets per cell from more than 50 cells were measured by ImageJ. A line was drawn along the maximum diameter in each individual lipid droplet and the diameters were ranked for size distribution analysis. The top three measurements were selected as the largest three lipid droplets in one cell. The images of peripheral lipid droplets were taken by focusing on the surface of the fat body cell. For antibody staining, fixed samples were washed in 0.1% PBST (Tween-20 diluted with PBS). Then, samples were blocked in 5% BSA (Sigma, diluted with 0.1% PBST) for 30 min at room temperature. After another wash in 0.1% PBST, samples were incubated with anti-GFP antibody (Abcam, diluted 1:10,000 with 0.1% PBST) at 4°C overnight. The fluorescent secondary antibody Rb488 was also diluted with 0.1% PBST. GFP knockin flies were used to examine the localization of fluorescent proteins on lipid droplets. The fluorescence intensity on the lipid droplet surface of 30 fat body cells was measured by ImageJ. For fluorescence intensity analysis, a line was plotted across a single lipid droplet. The fluorescence intensity value along the line was recorded. The peak in the curve represents the fluorescence intensity value on the lipid droplet surface. The fluorescence intensity results were normalized to the cytosolic intensity. The images were obtained by a Leica TCS SP8 and a LSM980 high-resolution confocal microscope.

Molecular biology and quantitative RT-PCR

For *pUAST-Flag-CG2064* and *pUAST-Flag-CG2064ATM*, the *CG2064* coding region was amplified from *Drosophila* cDNA and inserted in frame into the *pUAST-attB-Flag* vector through the NotI and XbaI sites. For *pUAST-CG2064-GFP*, the *CG2064* coding region (without the stop codon) was amplified and inserted in frame into the *pUAST-attB-GFP* vector through the NotI and KpnI sites. For *pUAST-CG2064^{N151L}*, *pUAST-CG2064^{Y204F}*, and *pUAST-CG2064^{K208A}*, site-direct mutagenesis was conducted by fusion PCR. For *pUAST-Plin1-GFP* and *pUAST-Plin2-GFP*, the *Plin1* or *Plin2* coding region (without the stop codon) was amplified and inserted in frame into the *pUAST-attB-GFP* vector through the NotI and KpnI sites. For *pUAST-Plin2-Plin1-C-GFP* and *pUAST-Plin1-C deletion*, the sequences of *Plin2-Plin1-C* and *Plin1-C deletion* (without the stop codon) were amplified and inserted in-frame into the *pUAST-attB-GFP* vector through the NotI and KpnI sites. *Plin2-Plin1-C* and *Plin1-C deletion* were first generated by PCR. All constructs were confirmed by sequencing. The efficiency of gene overexpression or knockdown was verified by quantitative RT-PCR. All quantitative RT-PCRs were performed on a Stratagene Mx3000P QPCR cyclor (Applied Biosystems) using Transstart Green qPCR super Mix kit (Transgen). The quantitative RT-PCR results were normalized with *rp49* gene.

Proteomic analysis

To identify the proteins downstream of CSN, 30 pairs of 3rd instar larval fat bodies were dissected in PBS buffer. Three biological repeats were performed for each genotype. Protein digestion with sequencing grade trypsin (Promega) was performed using the filter-aided proteome preparation (FASP) method. Resultant tryptic peptides were labeled with acetonitrile-dissolved TMT reagents (Thermo Fisher Scientific). Equal amounts of labeled samples were mixed together before prefractionation with reversed phase (RP)-high

performance liquid chromatography (HPLC). The peptides were fractionated on a Phenomenex Gemini-NX 5 u C18 column (250 × 3.0 mm, 110 Å, Torrance) with a Waters e2695 separations HPLC system. All samples were dried with a Speed-Vac concentrator and desalted by StageTip before use. The LC-MS/MS analysis was performed with an LTQ Orbitrap Elite mass spectrometer (Thermo Fisher Scientific) coupled online to an Easy-nLC 1,000 in the data-dependent mode. The peptides were injected into a capillary analytic column (length: 25 cm and inner diameter: 75 μm) packed with C18 particles (diameter: 5 μm). The positive ion mode was used for MS measurements. The spectra were acquired across the mass range of 300–1,800 *m/z*. The database search was performed for all raw MS files with MaxQuant (version 1.5).

To identify RDH/CG2064 interacting partners, 100 pairs of 3rd instar larval fat bodies of *RDH/CG2064-GFP*-overexpressing line were dissected in cold PBS buffer and homogenized on ice in RIPA buffer. The cell lysate was spun at 16,060 *g* for 15 min at 4°C to remove the cellular debris. The supernatant was incubated with anti-GFP affinity beads (Sigma-Aldrich) at 4°C overnight. Subsequently, the beads were washed three times with RIPA buffer. The eluted proteins were then digested with trypsin then for MS analyses with an LTQ Orbitrap Elite mass spectrometer (Thermo Fisher Scientific) coupled online to an Easy-nLC 1000 (Thermo Fisher Scientific) in the data-dependent mode.

Western blot and quantification

Drosophila S2 cells were cultured with Sf-900 II serum-free medium (GIBCO) at 26°C. The overexpression plasmid and the *actin-GAL4* plasmid were transfected into S2 cells with Cellfectin II (Invitrogen) or PLUS reagent (Invitrogen). Forty-eight hours after transfection, the cells were treated with DMSO or 40 μM proteasome inhibitor MG132 (Sigma-Aldrich) for 7 h. After removing the medium, cells were lysed with radioimmunoprecipitation assay (RIPA) buffer for 20 min on ice. The lysates were centrifuged at 13,680 *g* for 10 min at 4°C. The supernatants were retained for SDS-PAGE and western blots.

For larval samples, 3rd instar larval fat bodies were dissected in PBS buffer, transferred to 200 μl cold 1% SDS lysis buffer, and homogenized with an electronic pestle. Samples were then centrifuged at 13,680 *g* for 15 min at 4°C. The supernatants were retained for SDS-PAGE and western blots. Ten 3rd instar larvae per group and three groups for each genotype were used.

For immunoprecipitation, 20 μl IP beads (Sigma-Aldrich) were pre-cleaned with lysis buffer by centrifuging at 860 *g* for 1 min at 4°C. This step was repeated three times. Lysates of cultured cells or larval samples were incubated with IP beads at 4°C overnight. Subsequently, the beads were washed three times with RIPA buffer. 60 μl 1x SDS-loading buffer (125 mM Tris-HCl, pH 6.8, 20% glycerol, 2% SDS, 0.05% bromophenol blue, 10% 2-mercaptoethanol) was added to the sample. The samples were boiled at 100°C for 10 min and centrifuged at 13,680 *g* for 2 min. The supernatant was kept for western blots. The antibodies for western blotting were anti-GFP (Abcam), anti-Flag (Sigma-Aldrich), and anti-α-tubulin (Sigma-Aldrich).

For cell fraction, 3rd instar larval fat bodies were dissected in PBS buffer. Larval fat body lysates were diluted with subcellular fraction buffer (250 mM sucrose, 20 mM HEPES, 10 mM KCl, 1.5 mM MgCl₂, 1 mM EDTA, 1 mM EGTA, and 1 mM DTT) to 5 mg/ml final protein concentration. The cytosolic fraction and the membrane

fraction were separated by super-speed centrifugation. The soluble (liquid) fraction contained the cytosolic protein and the precipitate contained the membranous fragment. The soluble fraction was concentrated from 1 ml to 40 μl. The precipitate was dissolved in 40 μl buffer.

Glyceride quantification

To measure glyceride content, fat bodies of wandering 3rd instar larvae were dissected in 200 μl PBST buffer and then transferred into liquid nitrogen. Glyceride quantification was performed based on previous study (Palanker *et al*, 2009). For total glyceride, ten 3rd instar larvae (three groups of ten for each genotype) were used. Glyceride level was measured using TAG determination kits (Zhongshengbeikong). Glyceride measurement was normalized by total protein level.

Starvation test

For oenocyte staining, fed and 6-h starved larvae were dissected and stained with Oil Red. To test the larval survival rate after starvation, embryos for testing were collected within 4 h and raised at low density on standard fly food at 25°C. Seventy-two hours after hatching, larvae were either fed with standard food or starved on PBS-soaked paper for 12, 24, 36, 48, and 60 h. For the survival assay, three groups of 60 larvae for each genotype were starved. Then larvae were transferred back to standard food. Survival rate is based on counting the number of surviving adult flies.

RNAi in S2 cell

Based on RNAi stock information from flybase (CSN2:BL28290, VDRCGD4682; CSN3:DRSC32997, CSN5:DRSC16592; and CSN7:DRSC06808), 300–500 bp dsRNA fragments of CSN genes were selected. Target dsDNA fragments were amplified by PCR using the T7 promoter. The PCR fragments were purified and extracted. dsDNA was transcribed to dsRNA using the T7 Ultra Kit (Life Technologies, AM1345). S2 cells were resuspended at 1 × 10⁶ cells/ml in serum-free medium and 1 ml cells was plated into each well of a 6-well tissue culture plate. 30 μg dsRNA were added to each well. The plates were incubated at room temperature for 30 min, before adding 3 ml complete media with 10% FBS to each well. The cells were incubated for 3 days for further analysis.

Pulse-chase experiments in S2 cells

To follow protein kinetics in S2 cells, RDH/CG2064-GFP or Bmm-GFP overexpression was driven by *actin-Gal4* by transfection at 1 × 10⁶ cells/ml in serum-free medium. To inhibit protein synthesis, cells were treated with 50 μM cycloheximide (Cayman) for different times (0.5–6 h). After 48 h overexpression, protein was extracted to measure the levels of RDH/CG2064 or BMM protein with or without CSN knockdown by western blot.

RDH/CG2064 and CG2065 deletion mutants

The *RDH/CG2064-CG2065* double knockout (DKO) mutant was generated by Cas9 precise excision (Qidong Fungene Biotechnology

Co., Ltd.). Cas9 excision leads to a 3-kb deletion, spanning the coding regions of the *RDH/CG2064* and *CG2065* genes.

Statistical analysis

Unless specified, all data are shown as mean \pm SEM. All the experiments were performed three times. Based on different types of data, statistical analyses were performed with Student's *t* test (two group comparison) or one-way ANOVA with a *post hoc* Tukey's multiple comparison test (> 2 group comparison). $**P < 0.001$, $*P < 0.01$, and $*P < 0.05$, ns: not significantly different.

Expanded View for this article is available online.

Acknowledgements

We thank Drs. Shilai Bao, Pingsheng Liu, Guanghou Shui, and Zhaohui Wang for providing reagents and helpful discussions. This research was supported by grants 2018YFA0506902, 91954207, 31630019, and 91857000 from the National Key R&D Program of China and the National Natural Science Foundation of China.

Author contributions

Xuefan Zhao: Conceptualization; Investigation; Writing – original draft. **Wei Wang:** Methodology. **Yan Yao:** Resources; Methodology. **Xia Li:** Formal analysis. **Xiahe Huang:** Methodology. **Yingchun Wang:** Supervision. **Mei Ding:** Supervision. **Xun Huang:** Conceptualization; Supervision; Writing – original draft; Project administration; Writing – review & editing.

In addition to the CRediT author contributions listed above, the contributions in detail are:

Experiments were designed by XZ and XH. Samples preparation and most experiments were done by XZ. IP of RDH/CG2064 interaction proteins was performed by WW. *Plin1*, *Plin2*, and *Bmm* Knock-in *Drosophila* was first analyzed by YY. *Drosophila* screen was performed by XL. Proteomic analysis was performed by XHH and YW. XZ, MD, and XH analyzed the results. XZ and XH wrote the manuscript.

Disclosure and competing interests statement

The authors declare that they have no conflict of interest.

References

- Adams MK, Belyaeva OV, Wu L, Kedishvili NY (2014) The retinaldehyde reductase activity of DHRS3 is reciprocally activated by retinol dehydrogenase 10 to control retinoid homeostasis. *J Biol Chem* 289: 14868–14880
- Bagchi R, Melnyk CW, Christ G, Winkler M, Kirchsteiner K, Salehin M, Mergner J, Niemeyer M, Schwachheimer C, Villalobos LIAC et al (2018) The *Arabidopsis* ALF4 protein is a regulator of SCF E3 ligases. *EMBO J* 37: 255–268
- Baumbach J, Hummel P, Bickmeyer I, Kowalczyk KM, Frank M, Knorr K, Hildebrandt A, Riedel D, Jackle H, Kuhnlein RP (2014) A *Drosophila* in vivo screen identifies store-operated calcium entry as a key regulator of adiposity. *Cell Metab* 19: 331–343
- Beller M, Bulankina AV, Hsiao HH, Urlaub H, Jackle H, Kuhnlein RP (2010) PERILIPIN-dependent control of lipid droplet structure and fat storage in *Drosophila*. *Cell Metab* 12: 521–532
- Belyaeva OV, Wu L, Shmarakov I, Nelson PS, Kedishvili NY (2018) Retinol dehydrogenase 11 is essential for the maintenance of retinol homeostasis in liver and testis in mice. *J Biol Chem* 293: 6996–7007
- Berry DC, Noy N (2009) All-trans-retinoic acid represses obesity and insulin resistance by activating both peroxisome proliferation-activated receptor beta/delta and retinoic acid receptor. *Mol Cell Biol* 29: 3286–3296
- Bi J, Xiang Y, Chen H, Liu Z, Gronke S, Kuhnlein RP, Huang X (2012) Opposite and redundant roles of the two *Drosophila* perilipins in lipid mobilization. *J Cell Sci* 125: 3568–3577
- Blanchette-Mackie EJ, Dwyer NK, Barber T, Coxey RA, Takeda T, Rondinone CM, Theodorakis JL, Greenberg AS, Londos C (1995) Perilipin is located on the surface layer of intracellular lipid droplets in adipocytes. *J Lipid Res* 36: 1211–1226
- Blaner WS, O'Byrne SM, Wongsitiroj N, Kluwe J, D'Ambrosio DM, Jiang H, Schwabe RF, Hillman EM, Piantadosi R, Libien J (2009) Hepatic stellate cell lipid droplets: a specialized lipid droplet for retinoid storage. *Biochim Biophys Acta* 1791: 467–473
- Chen L, Chen XW, Huang X, Song BL, Wang Y, Wang Y (2019) Regulation of glucose and lipid metabolism in health and disease. *Sci China Life Sci* 62: 1420–1458
- Craney A, Rape M (2013) Dynamic regulation of ubiquitin-dependent cell cycle control. *Curr Opin Cell Biol* 25: 704–710
- Deisenroth C, Itahana Y, Tollini L, Jin A, Zhang Y (2011) p53-Inducible DHRS3 is an endoplasmic reticulum protein associated with lipid droplet accumulation. *J Biol Chem* 286: 28343–28356
- Diaconeasa B, Mazock GH, Mahowald AP, Dubreuil RR (2013) Genetic studies of spectrin in the larval fat body of *Drosophila melanogaster*: evidence for a novel lipid uptake apparatus. *Genetics* 195: 871–881
- Ding L, Yang X, Tian H, Liang J, Zhang F, Wang G, Wang Y, Ding M, Shui G, Huang X (2018) Seipin regulates lipid homeostasis by ensuring calcium-dependent mitochondrial metabolism. *EMBO J* 37: e97572
- Fan W, Lam SM, Xin J, Yang X, Liu Z, Liu Y, Wang Y, Shui G, Huang X (2017) *Drosophila* TRF2 and TAF9 regulate lipid droplet size and phospholipid fatty acid composition. *PLoS Genet* 13: e1006664
- Farese Jr RV, Walther TC (2009) Lipid droplets finally get a little R-E-S-P-E-C-T. *Cell* 139: 855–860
- Fei W, Shui G, Zhang Y, Krahmer N, Ferguson C, Kapterian TS, Lin RC, Dawes IW, Brown AJ, Li P et al (2011) A role for phosphatidic acid in the formation of "supersized" lipid droplets. *PLoS Genet* 7: e1002201
- Gluchowski NL, Becuwe M, Walther TC, Farese Jr RV (2017) Lipid droplets and liver disease: from basic biology to clinical implications. *Nat Rev Gastroenterol Hepatol* 14: 343–355
- Gong J, Sun Z, Wu L, Xu W, Schieber N, Xu D, Shui G, Yang H, Parton RG, Li P (2011) Fsp27 promotes lipid droplet growth by lipid exchange and transfer at lipid droplet contact sites. *J Cell Biol* 195: 953–963
- Granneman JG, Moore HP, Krishnamoorthy R, Rathod M (2009) Perilipin controls lipolysis by regulating the interactions of AB-hydrolase containing 5 (Abhd5) and adipose triglyceride lipase (Atgl). *J Biol Chem* 284: 34538–34544
- Greenberg AS, Egan JJ, Wek SA, Garty NB, Blanchette-Mackie EJ, Londos C (1991) Perilipin, a major hormonally regulated adipocyte-specific phosphoprotein associated with the periphery of lipid storage droplets. *J Biol Chem* 266: 11341–11346
- Gronke S, Beller M, Fellert S, Ramakrishnan H, Jackle H, Kuhnlein RP (2003) Control of fat storage by a *Drosophila* PAT domain protein. *Curr Biol* 13: 603–606
- Gronke S, Mildner A, Fellert S, Tennagels N, Petry S, Muller G, Jackle H, Kuhnlein RP (2005) Brummer lipase is an evolutionary conserved fat storage regulator in *Drosophila*. *Cell Metab* 1: 323–330

- Gronke S, Muller G, Hirsch J, Fellert S, Andreou A, Haase T, Jackle H, Kuhnlein RP (2007) Dual lipolytic control of body fat storage and mobilization in *Drosophila*. *PLoS Biol* 5: e137
- Guo Y, Walther TC, Rao M, Stuurman N, Goshima G, Terayama K, Wong JS, Vale RD, Walter P, Farese RV (2008) Functional genomic screen reveals genes involved in lipid-droplet formation and utilization. *Nature* 453: 657–661
- Hermes A, Bosch M, Ariotti N, Reddy B, Fajardo A, Fernández-Vidal A, Alvarez-Guaita A, Fernández-Rojo M, Rentero C, Tebar F et al (2013) Cell-to-cell heterogeneity in lipid droplets suggests a mechanism to reduce lipotoxicity. *Curr Biol* 23: 1489–1496
- Jiang W, Napoli JL (2013) The retinol dehydrogenase Rdh10 localizes to lipid droplets during acyl ester biosynthesis. *J Biol Chem* 288: 589–597
- Jornvall H, Persson B, Krook M, Atrian S, Gonzalez-Duarte R, Jeffery J, Ghosh D (1995) Short-chain dehydrogenases/reductases (SDR). *Biochemistry* 34: 6003–6013
- Keller B, Adamski J (2007) RDH12, a retinol dehydrogenase causing Leber's congenital amaurosis, is also involved in steroid metabolism. *J Steroid Biochem Mol Biol* 104: 190–194
- Kimmel AR, Sztalryd C (2016) The Perilipins: major cytosolic lipid droplet-associated proteins and their roles in cellular lipid storage, mobilization, and systemic homeostasis. *Annu Rev Nutr* 36: 471–509
- Kong J, Ji Y, Jeon YG, Han JS, Han KH, Lee JH, Lee G, Jang H, Choe SS, Baes M et al (2020) Spatiotemporal contact between peroxisomes and lipid droplets regulates fasting-induced lipolysis via PEX5. *Nat Commun* 11: 578
- Krahmer N, Farese Jr RV, Walther TC (2013) Balancing the fat: lipid droplets and human disease. *EMBO Mol Med* 5: 973–983
- Li S, Li Q, Kong Y, Wu S, Cui Q, Zhang M, Zhang SO (2017) Specific regulation of thermosensitive lipid droplet fusion by a nuclear hormone receptor pathway. *Proc Natl Acad Sci USA* 114: 8841–8846
- Listenberger LL, Ostermeyer-Fay AG, Goldberg EB, Brown WJ, Brown DA (2007) Adipocyte differentiation-related protein reduces the lipid droplet association of adipose triglyceride lipase and slows triacylglycerol turnover. *J Lipid Res* 48: 2751–2761
- Liu Y, Wang W, Shui G, Huang X (2014) CDP-diacylglycerol synthetase coordinates cell growth and fat storage through phosphatidylinositol metabolism and the insulin pathway. *PLoS Genet* 10: e1004172
- Min KW, Hwang JW, Lee JS, Park Y, Tamura TA, Yoon JB (2003) TIP120A associates with cullins and modulates ubiquitin ligase activity. *J Biol Chem* 278: 15905–15910
- Miura S, Gan JW, Brzostowski J, Parisi MJ, Schultz CJ, Londos C, Oliver B, Kimmel AR (2002) Functional conservation for lipid storage droplet association among Perilipin, ADRP, and TIP47 (PAT)-related proteins in mammals, *Drosophila*, and dictyostelium. *J Biol Chem* 277: 32253–32257
- Miyoshi H, Perfield 2nd JW, Souza SC, Shen WJ, Zhang HH, Stancheva ZS, Kraemer FB, Obin MS, Greenberg AS (2007) Control of adipose triglyceride lipase action by serine 517 of perilipin a globally regulates protein kinase A-stimulated lipolysis in adipocytes. *J Biol Chem* 282: 996–1002
- Molenaar MR, Vaandrager AB, Helms JB (2017) Some lipid droplets are more equal than others: different metabolic lipid droplet pools in hepatic stellate cells. *Lipid Insights* 10: 1178635317747281
- Mosher J, Zhang W, Blumhagen RZ, D'Alessandro A, Nerrikov T, Hansen KC, Hesselberth JR, Reis T (2015) Coordination between *Drosophila* Arc1 and a specific population of brain neurons regulates organismal fat. *Dev Biol* 405: 280–290
- Pacia MZ, Majzner K, Czamara K, Sternak M, Chlopicki S, Baranska M (2020) Estimation of the content of lipids composing endothelial lipid droplets based on Raman imaging. *Biochim Biophys Acta Mol Cell Biol Lipids* 1865: 158758
- Palanker L, Tennesen JM, Lam G, Thummel CS (2009) *Drosophila* HNF4 regulates lipid mobilization and beta-oxidation. *Cell Metab* 9: 228–239
- Pierce NW, Lee JE, Liu X, Sweredoski MJ, Graham RLJ, Larimore EA, Rome M, Zheng N, Clurman BE, Hess S et al (2013) Cand1 promotes assembly of new SCF complexes through dynamic exchange of F Box proteins. *Cell* 153: 206–215
- Rinia HA, Burger KN, Bonn M, Muller M (2008) Quantitative label-free imaging of lipid composition and packing of individual cellular lipid droplets using multiplex CARS microscopy. *Biophys J* 95: 4908–4914
- Ruggles KV, Turkish A, Sturley SL (2013) Making, baking, and breaking: the synthesis, storage, and hydrolysis of neutral lipids. *Annu Rev Nutr* 33: 413–451
- Sandell LL, Sanderson BW, Moiseyev G, Johnson T, Mushegian A, Young K, Rey JP, Ma JX, Staehling-Hampton K, Trainor PA (2007) RDH10 is essential for synthesis of embryonic retinoic acid and is required for limb, craniofacial, and organ development. *Genes Dev* 21: 1113–1124
- Schwechheimer C, Serino G, Callis J, Crosby WL, Lyapina S, Deshaies RJ, Gray WM, Estelle M, Deng XW (2001) Interactions of the COP9 signalosome with the E3 ubiquitin ligase SCFTIR1 in mediating auxin response. *Science* 292: 1379–1382
- Siddiqah IM, Manandhar SP, Cocca SM, Hsueh T, Cervantes V, Gharakhanian E (2017) Yeast ENV9 encodes a conserved lipid droplet (LD) short-chain dehydrogenase involved in LD morphology. *Curr Genet* 63: 1053–1072
- Sinha A, Israeli R, Cirigliano A, Gihaz S, Trabelcy B, Braus GH, Gerchman Y, Fishman A, Negri R, Rinaldi T et al (2020) The COP9 signalosome mediates the Spt23 regulated fatty acid desaturation and ergosterol biosynthesis. *FASEB J* 34: 4870–4889
- Su W, Wang Y, Jia X, Wu W, Li L, Tian X, Li S, Wang C, Xu H, Cao J et al (2014) Comparative proteomic study reveals 17beta-HSD13 as a pathogenic protein in nonalcoholic fatty liver disease. *Proc Natl Acad Sci USA* 111: 11437–11442
- Sun Z, Gong J, Wu H, Xu W, Wu L, Xu D, Gao J, Wu J-W, Yang H, Yang M et al (2013) Perilipin1 promotes unilocular lipid droplet formation through the activation of Fsp27 in adipocytes. *Nat Commun* 4: 1594
- Ugrankar R, Bowerman J, Hariri H, Chandra M, Chen K, Bossanyi M-F, Datta S, Rogers S, Eckert KM, Vale G et al (2019) *Drosophila* Snazarus regulates a lipid droplet population at plasma membrane-droplet contacts in adipocytes. *Dev Cell* 50: 557–572
- Walther TC, Farese Jr RV (2012) Lipid droplets and cellular lipid metabolism. *Annu Rev Biochem* 81: 687–714
- Wang H, Sreenivasan U, Hu H, Saladino A, Polster BM, Lund LM, Gong DW, Stanley WC, Sztalryd C (2011) Perilipin 5, a lipid droplet-associated protein, provides physical and metabolic linkage to mitochondria. *J Lipid Res* 52: 2159–2168
- Welte MA (2015) Expanding roles for lipid droplets. *Curr Biol* 25: R470–R481
- Welte MA, Cermelli S, Griner J, Viera A, Guo Y, Kim DH, Gindhart JG, Gross SP (2005) Regulation of lipid-droplet transport by the perilipin homolog LSD2. *Curr Biol* 15: 1266–1275
- Wilfling F, Wang H, Haas J, Krahmer N, Gould T, Uchida A, Cheng J-X, Graham M, Christiano R, Fröhlich F et al (2013) Triacylglycerol synthesis enzymes mediate lipid droplet growth by relocating from the ER to lipid droplets. *Dev Cell* 24: 384–399
- Xie Y, Lee W, Cai C, Gambin T, Nöpuu K, Sujirakul T, Ayuso C, Jhangiani S, Muzny D, Boerwinkle E et al (2014) New syndrome with retinitis

- pigmentosa is caused by nonsense mutations in retinol dehydrogenase RDH11. *Hum Mol Genet* 23: 5774–5780
- Yang D, Vuckovic MG, Smullin CP, Kim M, Lo CP, Devericks E, Yoo HS, Tintcheva M, Deng Y, Napoli JL (2018) Modest decreases in endogenous all-trans-retinoic acid produced by a mouse Rdh10 heterozygote provoke major abnormalities in adipogenesis and lipid metabolism. *Diabetes* 67: 662–673
- Yao Y, Li X, Wang W, Liu Z, Chen J, Ding M, Huang X (2018) MRT, functioning with NURF complex, regulates lipid droplet size. *Cell Rep* 24: 2972–2984
- Yoshizawa T, Karim M, Sato Y, Senokuchi T, Miyata K, Fukuda T, Go C, Tasaki M, Uchimura K, Kadomatsu T *et al* (2014) SIRT7 controls hepatic lipid metabolism by regulating the ubiquitin-proteasome pathway. *Cell Metab* 19: 712–721
- Yu J, Li P (2017) The size matters: regulation of lipid storage by lipid droplet dynamics. *Sci China Life Sci* 60: 46–56
- Zimmermann R, Strauss JG, Haemmerle G, Schoiswohl G, Birner-Gruenberger R, Riederer M, Lass A, Neuberger G, Eisenhaber F, Hermetter A *et al* (2004) Fat mobilization in adipose tissue is promoted by adipose triglyceride lipase. *Science* 306: 1383–1386



License: This is an open access article under the terms of the Creative Commons Attribution-NonCommercial-NoDerivs License, which permits use and distribution in any medium, provided the original work is properly cited, the use is non-commercial and no modifications or adaptations are made.